SIGNAL ENHANCEMENT OF SPECULARLY SCATTERED UNDERWATER SOUND

Robert Bishop Shields

NAVAL POSTGRADUATE SCHOOL
Monterey, California

THESIS

SIGNAL ENHANCEMENT OF SPECULARLY SCATTERED UNDERWATER SOUND

by

Robert Bishop Shields, Jr.

December 1977

Thesis Advisor: H. Medwin

REPORT DOCUMENTATION PAGE

READ INSTRUCTIONS BEFORE COMPLETING FORM

1. REPORT NUMBER	2. GOVT ACCESSION NO. / 3. RECIPIENT'S CATALOG NUMBER
4. TITLE (and Subtitle): Signal Enhancement of Specularly Scattered Underwater Sound	5. TYPE OF REPORT & PERIOD COVERED: Master's Thesis; December 1977
	6. PERFORMING ORG. REPORT NUMBER
7. AUTHOR(s): Robert Bishop Shields, Jr.	8. CONTRACT OR GRANT NUMBER(s)
9. PERFORMING ORGANIZATION NAME AND ADDRESS: Naval Postgraduate School, Monterey, California 93940	10. PROGRAM ELEMENT, PROJECT, TASK AREA & WORK UNIT NUMBERS
11. CONTROLLING OFFICE NAME AND ADDRESS: Naval Postgraduate School, Monterey, California 93940	12. REPORT DATE: December 1977
	13. NUMBER OF PAGES: 92
14. MONITORING AGENCY NAME & ADDRESS(if different from Controlling Office)	15. SECURITY CLASS. (of this report): Unclassified
	15a. DECLASSIFICATION/DOWNGRADING SCHEDULE

16. DISTRIBUTION STATEMENT (of this Report)

Approved for public release; distribution unlimited.

17. DISTRIBUTION STATEMENT (of the abstract entered in Block 20, if different from Report)

18. SUPPLEMENTARY NOTES

19. KEY WORDS (Continue on reverse side if necessary and identify by block number)

Specularly scattered underwater sound

20. ABSTRACT (Continue on reverse side if necessary and identify by block number)

The wind driven surface of a model ocean was used to study the simultaneous amplitude fluctuations of 31 specularly scattered harmonic components from 5 kHz - 150 kHz. The temporal variations of the scattered components show maxima and minima whose anticorrelation depends on the sound frequency ratio . Significant signal enhancement can be obtained through timely frequency switching between a base

(20. ABSTRACT Continued)

frequency and its second harmonic. This gain is found to depend on the effective surface roughness, $g^{\frac{1}{2}} = \frac{4\pi\sigma}{\lambda} \cos\theta$ (where σ = RMS wave height and θ = angle of incidence), the duration of the experiment, and the switching threshold. For example, for a switching threshold 3 dB below the mean amplitude of the base frequency, the gain is about 5 dB at $g^{\frac{1}{2}} = 0.25$ and approximately 3 dB for $1 \leq g^{\frac{1}{2}} \leq 2$. This was the average gain observed for runs lasting for five ocean surface wave periods. Using only the coherent component of the signals provides greater gain for the higher roughnesses ($1.35 \leq g^{\frac{1}{2}} \leq 2.0$).

Approved for public release; distribution unlimited.

Signal Enhancement of Specularly Scattered Underwater Sound

by

Robert Bishop Shields, Jr.
Lieutenant, United States Navy
B.S., U.S. Naval Academy, 1972

Submitted in partial fulfillment of the requirements for the degree of

MASTER OF SCIENCE IN ENGINEERING ACOUSTICS

from the

NAVAL POSTGRADUATE SCHOOL
December 1977

ABSTRACT

The wind driven surface of a model ocean was used to study the simultaneous amplitude fluctuations of 31 specularly scattered harmonic components from 5 kHz - 160 kHz. The temporal variations of the scattered components show maxima and minima whose anticorrelation depends on the sound frequency ratio. Significant signal enhancement can be obtained through timely frequency switching between a base frequency and its second harmonic. This gain is found to depend on the effective surface roughness, $g^{\frac{1}{2}} = \frac{4\pi\sigma}{\lambda} \cos\theta$ (where σ = RMS wave height and θ = angle of incidence), the duration of the experiment, and the switching threshold. For example, for a switching threshold 3 dB below the mean amplitude of the base frequency, the gain is about 5 dB at $g^{\frac{1}{2}} = 0.25$ and approximately 3 dB for $1 \leq g^{\frac{1}{2}} \leq 2$. This was the average gain observed for runs lasting for five ocean surface wave periods. Using only the coherent component of the signals provides greater gain for the higher roughnesses ($1.35 \leq g^{\frac{1}{2}} \leq 2.0$).

TABLE OF CONTENTS

I. INTRODUCTION ---------- 9

A. OBJECTIVES ---------- 10

B. INTERMEDIATE GOALS ---------- 11

II. RESEARCH FACILITIES ---------- 13

A. OCEAN ACOUSTIC WAVE FACILITY ---------- 13

B. DATA ACQUISITION AND PROCESSING CAPABILITIES -- 16

C. STANDARD EQUIPMENT LIST ---------- 17

III. THEORY ---------- 19

IV. EXPERIMENTAL PROCEDURES ---------- 25

A. SOUND SOURCE AND RECEIVER SELECTION AND TESTING ---------- 25

B. SURFACE REFLECTED, PULSED SOUND ANALYSIS ------ 26

C. ELECTRICAL AND MECHANICAL STABILITY ANALYSIS -- 33

V. EXPERIMENTAL RESULTS AND ANALYSIS ---------- 37

A. INITIAL LOOK AT SPECULARLY SCATTERED SOUND ---- 37

B. EXAMINATION OF PHASE AND AMPLITUDE VARIATIONS - 41

C. SEPARATION OF THE COHERENT COMPONENT ---------- 43

D. INTERFREQUENCY CORRELATION VS. DELTA FREQUENCY ---------- 52

E. INTERFREQUENCY COVARIANCE VS. FREQUENCY RATIO - 57

F. SHORT TERM VARIABILITY OF RMS WAVE HEIGHT ----- 68

G. SIGNAL ENHANCEMENT DUE TO FREQUENCY SWITCHING - 74

H. RESULTS AND CONCLUSIONS ---------- 81

VI. RECOMMENDATIONS FOR FUTURE RESEARCH ---------- 83

APPENDIX A: COMPUTER PROGRAM DESCRIPTIONS ---------- 84

BIBLIOGRAPHY ---------- 90

INITIAL DISTRIBUTION LIST ---------- 91

LIST OF FIGURES

FIGURE 1 TOP VIEW OF OAWF ---------- 14

FIGURE 2 SIDE VIEW OF OAWF ---------- 15

FIGURE 3 RELECTION FROM A DETERMINISTIC SURFACE ----- 20

FIGURE 4 SPECULAR SCATTER FROM A RANDOMLY ROUGH SURFACE ---------- 20

FIGURE 5 EXPERIMENTAL SETUP ---------- 27

FIGURE 6 ANALYSIS OF SURFACE REFLECTED PULSE -------- 30

FIGURE 7 ANALYSIS OF DIRECT PATH PULSE ---------- 30

FIGURE 8 SOURCE "RINGING" ---------- 31

FIGURE 9 SERIES OF PULSES AND REFECTIONS ---------- 31

FIGURE 10 SIMULTANEOUS PRESSURE AMPLITUDE VS. TIME FOR 31 FREQUENCIES ---------- 38

FIGURE 11 PHASE HISTOGRAM AT 15 KHZ ---------- 44

FIGURE 12 PHASE HISTOGRAM AT 40 KHZ ---------- 45

FIGURE 13 PHASE HISTOGRAM AT 125 KHZ ---------- 46

FIGURE 14 AMPLITUDE HISTOGRAM AT 30 KHZ ---------- 47

FIGURE 15 AMPLITUDE HISTOGRAM AT 120 KHZ ---------- 48

FIGURE 16 AMPLITUDE HISTOGRAM AT 155 KHZ ---------- 49

FIGURE 17a INSTANTANEOUS RECEIVED SIGNAL ---------- 51

FIGURE 17b COHERENT COMPONENT ---------- 51

FIGURE 18 INTERFREQUENCY CORRELATION VS. DELTA FREQUENCY. TWO SECOND RUN ---------- 55

FIGURE 19 INTERFREQUENCY CORRELATION VS. DELTA FREQUENCY. 160 MSEC. RUN ---------- 56

FIGURE 20 SPECULAR REFLECTION FROM A SINUSOIDAL SURFACE ---------- 58

FIGURE 21 INTERFREQUENCY COVARIANCE VS. FREQUENCY RATIO. ANGLE OF INCIDENCE 32.6° ---------- 63

FIGURE 22 INTERFREQUENCY COVARIANCE VS. FREQUENCY RATIO. ANGLE OF INCIDENCE 66.1° ---------- 64

FIGURE 23 INTERFREQUENCY COVARIANCE VS. FREQUENCY RATIO. SWITCHING THRESHOLD MEAN OF F_1 ----- 65

FIGURE 24 INTERFREQUENCY COVARIANCE VS. FREQUENCY RATIO. SWITCHING THRESHOLD 3 DB BELOW MEAN OF F_1 ---------- 66

FIGURE 25 LN $\frac{<P>}{P_o}$ VS. (FREQUENCY)^2 FOR FIVE TWO SECOND RUNS ---------- 70

FIGURE 26 WAVE HEIGHT DATA COLLECTING CIRCUIT -------- 71

FIGURE 27 WAVE HEIGHT VS. TIME. SMALL AMPLITUDE ----- 72

FIGURE 28 WAVE HEIGHT VS. TIME. LARGE AMPLITUDE ----- 72

FIGURE 29 LN $\frac{<P>}{P_o}$ VS. (FREQUENCY)^2 FOR FIVE, SIX SECOND RUNS ---------- 73

FIGURE 30 GAIN VS. $(G)^{\frac{1}{2}}$ FOR TWELVE, TWO SECOND RUNS - 76

FIGURE 31 GAIN VS. $(G)^{\frac{1}{2}}$ FOR FIVE OCEAN PERIODS AND FIFTEEN OCEAN PERIODS ---------- 77

FIGURE 32 GAIN VS. $(G)^{\frac{1}{2}}$ FOR COHERENT VOLTAGES AND TOTAL VOLTAGES ---------- 79

FIGURE 33 GAIN VS. $(G)^{\frac{1}{2}}$ FOR SWITCHING THRESHOLD OF MEAN AND 3 DB BELOW MEAN ---------- 80

I. INTRODUCTION

The long term, statistical behavior of sound which is forward scattered from a rough surface has been well studied (Refs. 1,2,3,4 and 5). Little is known, however, of the short term variability of acoustic signals reflecting from statistically rough surfaces. "Short term" in this paper is defined as on the order of several ocean surface wave periods.

The "building and fading" of acoustic signals in the sea has been observed for decades. This phenomenon has been variously attributed to time-varying surface and/or bottom interference, internal waves and thermal gradients for example. Regardless of the source, the fading is especially troublesome in underwater communications and in the detection of undersea objects. Much effort has been directed toward the elimination of all but the direct path, relatively stable signal, in the oceans.

The aim of this work is to show that the fluctuations of sound caused by surface specular scattering are to some extent predictable. Thus the energy associated with these signals, normally discarded, can be utilized. Other authors have searched in this direction. Perkins (Ref. 6) showed that the spectrum of the modulation of the sum of the surface reflected and direct path signals was exactly that of the surface wave height spectrum and that signals stronger than

the average will recur for 3 to 5 cycles of the principle ocean period. Tourville (Ref. 7) showed that the surface reflected signal could always be constructively added to the direct path signal through the use of two directional receivers, a suitable delay network and knowledge of the surface wave height spectrum. Loomis (Ref. 8) further specialized by looking only at the surface reflected signal in the specular direction. He simultaneously examined many frequencies from a harmonically rich signal which was pulsed and received by a gating network. Loomis suggested that for a given RMS surface wave height there is a constant frequency separation between instantaneous amplitude maxima at one surface reflected frequency and minima at another such frequency. If so, this could be useful in detection or communication. One could switch to another frequency, predicted by Loomis' frequency separation idea, that would be reaching an amplitude maximum while the primary frequency was heading for an amplitude minimum.

This work is a continuation of Loomis' search for a predictable, instantaneous relationship among several frequencies simultaneously scattered from a rough surface.

A. OBJECTIVES

One objective of the research is to investigate the effect that variation of frequency has on the sound scattered from a statistically rough, fluctuating, wind driven water surface. Another objective is to determine if a predictable

relationship exists between the intensities of various harmonics of a sound source when scattered from such a surface. The basic requirements of this experimental research are:

1. Insonification of the fluctuating surface with many frequencies simultaneously,

2. Isolation of the surface reflected sound from other paths through the use of gated signals.

B. INTERMEDIATE GOALS

1. Locate an acoustic source that is capable of transmitting over a wide range of frequencies, is small enough to be considered a point source and yet has a significant output at 5 kHz. This last requirement was imposed in order to lower the fundamental frequency from Loomis' 10 kHz and thus improve the resolution.

2. Improve the mechanical setup and electronic circuitry in order to increase the stability of the experiment. The circuitry must still be capable of transmitting simultaneously a wide range of frequencies, receiving and processing these signals.

3. Develop a method of looking either at the coherent component or the total reflected signal.

4. Develop and implement computer programs to objectively analyze the data, ascertain any relationships among the frequencies and determine any improvement to be gained by timely frequency switching.

5. Vary the geometry to determine any dependence on angle of incidence.

6. Vary the duration of runs to determine any time dependence.

II. RESEARCH FACILITIES

A. OCEAN ACOUSTIC WAVE FACILITY (OAWF)

The Ocean Acoustic Wave Facility is a combination of a wind generated wave tunnel and an anechoic acoustic tank. The wind tunnel is approximately 17 meters long, 1.2 meters wide and 1.2 meters deep. By varying the number of fans and/or the distance between the water surface and the top of the tunnel, a wide range of ocean surfaces can be obtained. Figures 1 and 2 (from Tourville) show the essential features of the OAWF.

The wave generation tunnel empties into a water filled tank with dimensions of 3 meters on each side. The wind generated waves are dissipated on a constructed beach to prevent interference from reflected waves. A Lucite divider is placed in the tank as shown in figure 1. This divider reduces the divergence of the sea surface upon leaving the tunnel and ensures that most of the wind generated energy is dissipated on the beach. The tank is constructed of 4" x 4" redwood posts, placed with corners facing outward. The combination of scattering and absorption provided by the redwood was fairly effective in reducing echoes. All remaining reflections were eliminated by gating as explained in a later section. Equipment was either positioned within the tank by the use of moveable racks or suspended from mounts in the ceiling.

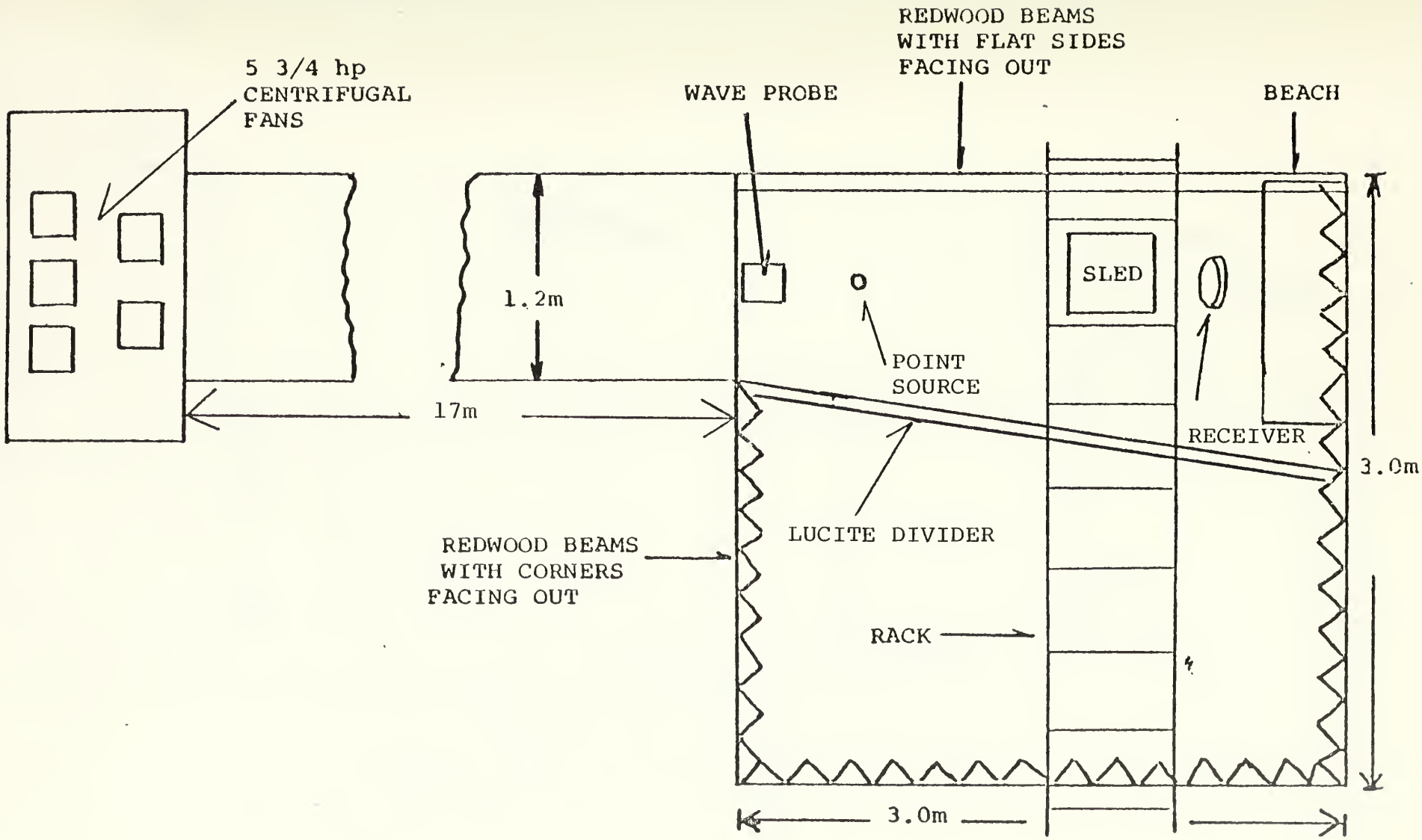

FIGURE 1. TOP VIEW of OAWF

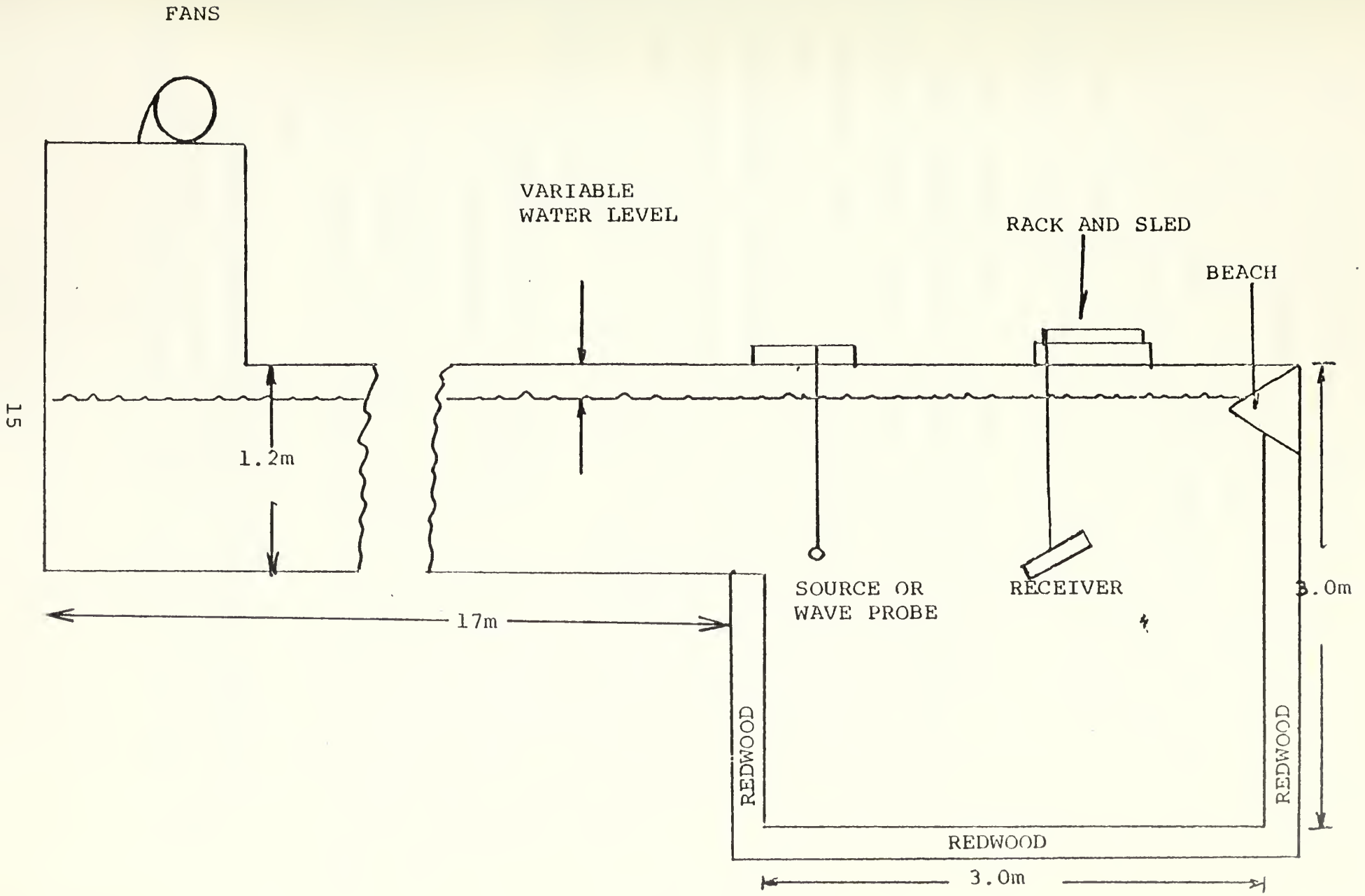

Figure 2. Side View of OAWF

The wind generated sea of OAWF has been compared with the real ocean in several ways over the past 10 years. It has been shown to be a suitable model in terms of the PDF of heights and slopes. It also compares well with, and is scaled to the two dimensional ocean wave number spectrum, the ocean frequency spectrum, and their transforms, the spatial and temporal correlation functions.

B. DATA ACQUISITION AND PROCESSING CAPABILITIES

Data acquisition and processing were accomplished by using a digital computer system composed of three primary components, each of which is interfaced to provide high speed analog to digital conversion, digital processing and data printout and recording. The design was developed by the Special Projects Section of the Naval Air Development Center in conjunction with Pinkerton Computer Consultants, Inc. of Warminster, Pennsylvania. The three components are described below:

1. Interdata Model 70 Computer

This minicomputer is a digital design that is FORTRAN and BASIC programmable with a 64 thousand byte memory. In addition to actual core memory, data that have been stored on digital cassettes can be read into the computer for processing.

2. Phoenix Analog to Digital Converters, Model ADC 712

Two ADC 712 analog to digital converters may be used separately or simultaneously. Each converter is a high speed

device capable of encoding ±10 volt input signals in digital form and providing an accuracy of 0.005 volts in 20 volts. The maximum sampling rate is 320,000 samples per second; this rate was used unless otherwise specified.

3. Texas Instruments Silent Electronic Data Terminal Model 733

The TI 733 consists of a keyboard used as a programming input/output control device, a printer, and a playback/record section used in conjunction with digital cassettes. The overall system facilitates rapid, accurate processing of any desired type of analog electrical signal and was used mainly for frequency domain and statistical analyses using standard FFT algorithms. Further descriptions are contained in References 6 and 7.

C. STANDARD EQUIPMENT LIST

A list of standard equipment referred to throughout the text is given below:

Abbreviation	Full Description
Scope	Tektronix Model 545B 4-channel oscilloscope
HP 466A Amp	Hewlett-Packard Voltage Amplifier Model 466A
HP 467A Amp	Hewlett-Packard Power Amplifier Model 467A
HP 218	Hewlett-Packard Model 218 Digital Delay Generator
HP 219	Hewlett-Packard Model 219 Dual Pulse Unit
KH 3332 Filter	Krohn-Hite Model 3332 Frequency Filter

KH 3550 Filter	Krohn-Hite Model 3550 Frequency Filter
Frequency Counter	Data Precision Model 5740 Frequency Counter
GR-1217C	General Radio Model 1217C Unit Pulse Generator
Impedance Bridge	General Radio Model 1650A Impedance Bridge
Wavetek 114	Wavetek Model 114 Function Generator
Wavetek 136	Wavetek Model 136 Function Generator
Wavetek 144	Wavetek Model 144 Function Generator
Wavetek 186	Wavetek Model 186 Function Generator

Sound sources, receivers, wave probes, and other miscellaneous equipment will be described in the text as necessary.

III. THEORY

A brief review of current scattering theory is appropriate. Chapter two of Beckmann and Spizzichino (Ref. 4) asks the question, "For what values of wavelength, surface roughness, and angle of incidence does specular reflection change into diffuse scattering ... when does a smooth surface become rough?" Consider for example figure 3. Rays 1 and 2 are incident on a surface with irregularities of height h at an angle of incidence α. The path difference between the two rays is:

$$\Delta r = 2\, h \cos \alpha$$

and the phase difference is:

$$\Delta\phi = 2\pi/\lambda\ \Delta r = \frac{4\pi h}{\lambda} \cos \alpha\ .$$

Now considering the surface displacement h to be varying randomly in time with RMS height σ, the variance of the phase difference is:

$$\text{Var}\ (\Delta\phi) = \left(\frac{4\pi}{\lambda} \cos \alpha\right)^2 \quad \text{Var}\ (h(t))$$

$$\text{Var}\ (\Delta\phi) = \left(\frac{4\pi\sigma}{\lambda} \cos \alpha\right)^2 = g_{\text{specular}}\ .$$

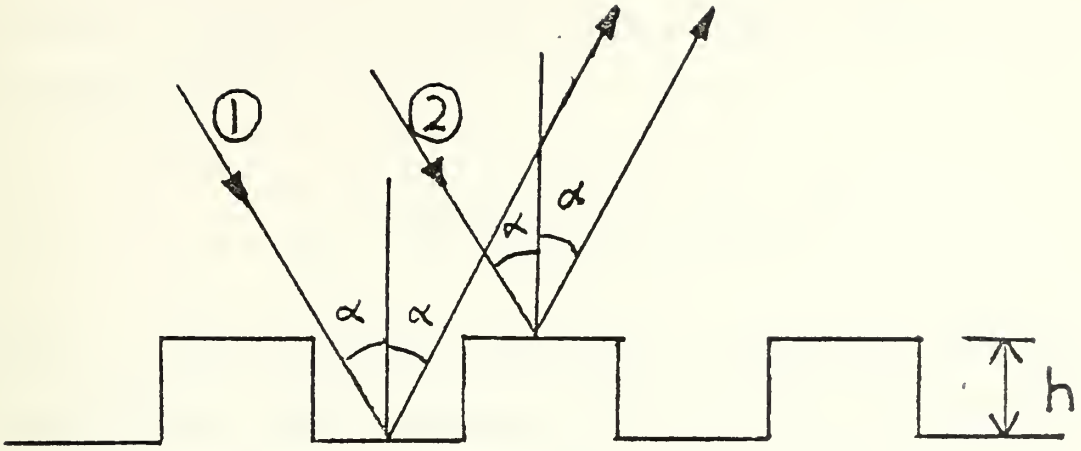

Figure 3. Reflection from a Deterministic Surface

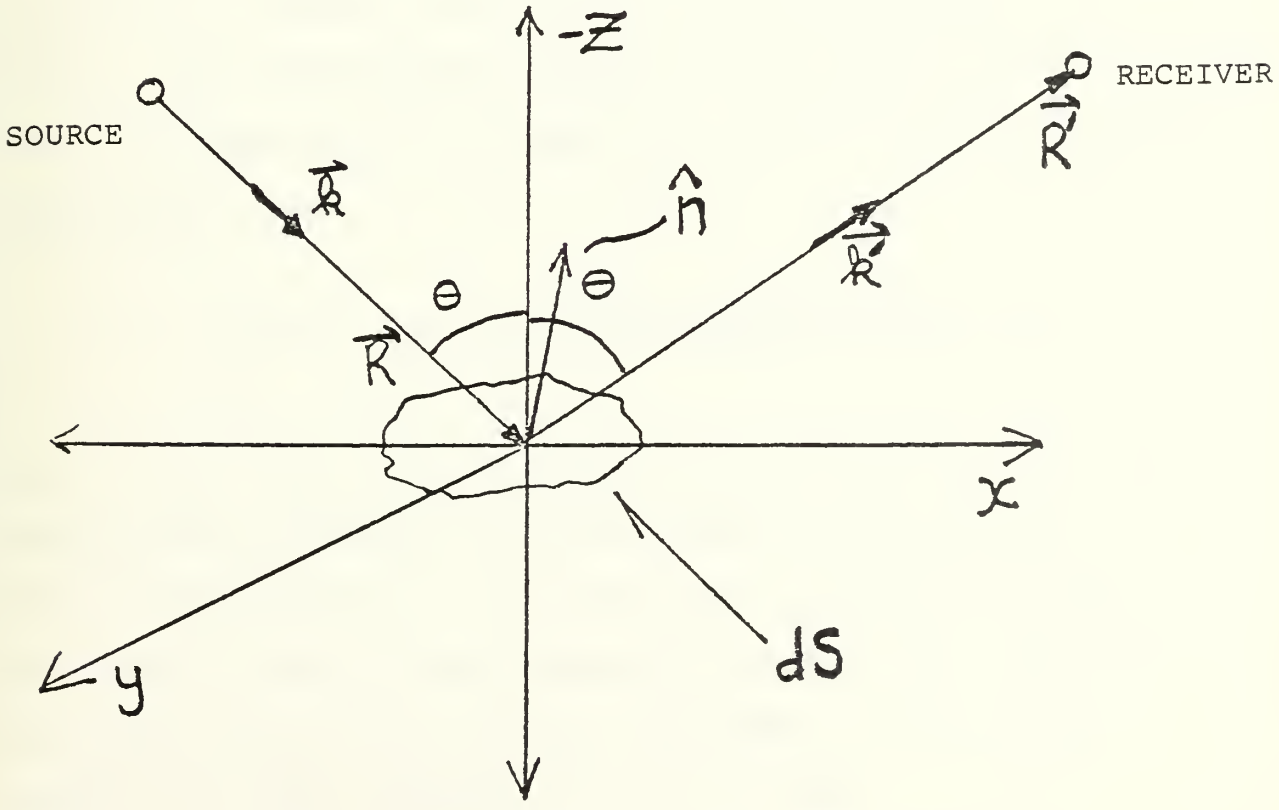

Figure 4. Specular Scatter from a Randomly Rough Surface

This quantity is known as the roughness parameter for specular scatter. In a more general form, the roughness parameter is:

$$g \equiv \left[\frac{2\pi\sigma}{\lambda}(\cos\theta_1 + \cos\theta_2)\right]^2$$

where θ_1 and θ_2 are the angles of incidence and reflection respectively. The description of the acoustical field in terms of g allows for comparison of data obtained from different surfaces, frequencies, and angles of incidence. The square root of g is the well known Rayleigh parameter which is often used instead of g.

Forward scattering is described in Ref. 1 and chapter 6 of Ref. 2. Figure 4 will aid in a recapitulation of the theory. The instantaneous pressure at any point in the field, with the aid of the Helmholtz theorem and the Kirchhoff approximation is:

$$p = \frac{1}{4\pi}e^{-i\omega t}\int_S R\ D\ \frac{\partial}{\partial n}\left\{\frac{\exp[i(\bar{k}\cdot\bar{R} + \bar{k}'\cdot\bar{R}')]}{R\ R'}\right\} dS$$

where $\bar{k}$ and $\bar{k}'$ are the wavenumbers along $\bar{R}$ and $\bar{R}'$, the radius vectors from the source to the scattering area and from there to the receiver. D is the source function including directivity, and R is the reflection coefficient. Expanding the radius vectors, and if the displacement of the rough surface z is small compared to R and R' then

$$k_z - k'_z \approx -2k\cos\theta \equiv 2\gamma$$

and finally taking the ensemble average of the signal, one arrives at:

$$\langle p \rangle \approx \frac{i\gamma}{2\pi} e^{i\omega t} \int_S R\, D \frac{\exp[ik(R_o + R'_o)]}{R_o R'_o} \langle e^{2i\gamma z} \rangle \, dS \ .$$

For the PDF, W of the surface, the average, over all values of z, is:

$$\langle e^{2i\gamma z} \rangle = \int_{-\infty}^{\infty} W e^{2i\gamma z} \, dz \ .$$

Defining p_o as the reflection from a mirror surface (z = 0) it follows:

$$\frac{\langle p \rangle}{p_o} \approx \int_{-\infty}^{\infty} W e^{2i\gamma z} \, dz \ .$$

If the rough surface has a Gaussian PDF then

$$\frac{\langle p \rangle}{p_o} \approx \exp(-2\gamma^2\sigma^2)$$

The roughness parameter g for specular scatter may be expressed as:

$$g = \left(\frac{4\pi\sigma}{\lambda}\cos\theta\right)^2 = 4\gamma^2\sigma^2$$

and therefore

$$\frac{\langle p \rangle}{p_o} \approx \exp\left(-\frac{g}{2}\right)$$

for a Gaussian PDF. Reference 2 points out that the above simplified relationship is good for non-Gaussian surfaces only when $g \leq 1$, and the incident ray is not near grazing.

The above relationship applies only to the coherent component of the scattered sound. The coherent component is defined in this paper as that component having a constant phase relationship or travelling a constant path length between source and receiver. Contributions at any instant from other paths are referred to as the incoherent component. Thus it is obvious that as a surface gets rougher, the coherent component will decrease and the incoherent component will increase. In an experiment one normally measures the total pressure $(pp^*)^{\frac{1}{2}}$ at any instant of time. Reference 3 gives a relationship between this measured total pressure and its two components:

$$\langle pp^* \rangle = \langle p \rangle^2 + S^2$$

where $\langle p \rangle^2$ is the square of the coherent component and S^2 is the variance of the pressure fluctuations, or the incoherent component. The point to all this is that when g is small, there is not much variation and the coherent component

dominates. As g or the apparent roughness increases, the incoherent starts to dominate.

IV. EXPERIMENTAL PROCEDURES

The experimental procedures followed in the course of this research can be grouped into three general categories: (A) Sound source and receiver selection and testing; (B) Surface reflected, pulsed sound analysis; (C) Electrical and mechanical stability analysis.

A. SOUND SOURCE AND RECEIVER SELECTION AND TESTING

Loomis (Ref. 8) utilized LC-10's for both source and receiver in his experiment. He also used 10 kHz and its harmonics up to 160 kHz for analysis. It was decided that 5 kHz would be used as the fundamental frequency in this experiment. With 160 kHz still the top frequency that could successfully be observed due to a maximum sampling rate of 320 kHz, the number of frequencies for analysis was doubled from 16 to 32. This gave twice the frequency resolution but it required a significant response from the source at 5 kHz. The following sources were tested:

a. LC-10 ceramic hydrophone
b. LC-32 ceramic hydrophone
c. a cylindrical ceramic transducer 4" in length and 1" in diameter
d. a 2" diameter ceramic sphere (Channelite 5400)
e. a .87" diameter ceramic sphere (Channelite 5400)
f. a .87" diameter ceramic sphere (Channelite 5400) with an external viscoelastic layer constrained by an epoxy coating

g. a .87" diameter ceramic sphere made with a material with a very low mechanical "Q" (Channelite 5550).

All of the above exhibited significant "ringing" at their resonance frequency. However, the resonance frequency of the "low Q" source was significantly lower than the others and it had a stronger output at 5 kHz and thus it was chosen.

Two receivers were tested, first Loomis' LC-10 and then an F-27. The major difference was that for the bandwidth considered, the LC-10 was omnidirectional while the F-27, which is a 27.3 cm. diameter piston, was quite directional. The beam width of the F-27 varies from 66° at 5 kHz to 2° at 125 kHz. Only signal reflected in the specular direction was desired for analysis. Since a directional receiver would be more successful in eliminating the incoherent component of the radiation which is that scattered from other than the specular direction, the F-27 was chosen.

B. SURFACE REFLECTED, PULSED SOUND ANALYSIS

Figure 5 is a schematic of the basic circuit used in the collection of all data. The geometry of the source and receiver was varied but the electrical setup remained constant throughout the experiment. The circuit is fairly similar to that of Loomis (Ref. 8). The differences will be explained in the next section on stability.

The heart of the setup is the Wavetek 144 function generator. It had been modified to given an asymmetrical sawtooth wave with a slope ratio of 44:1. A sawtooth wave

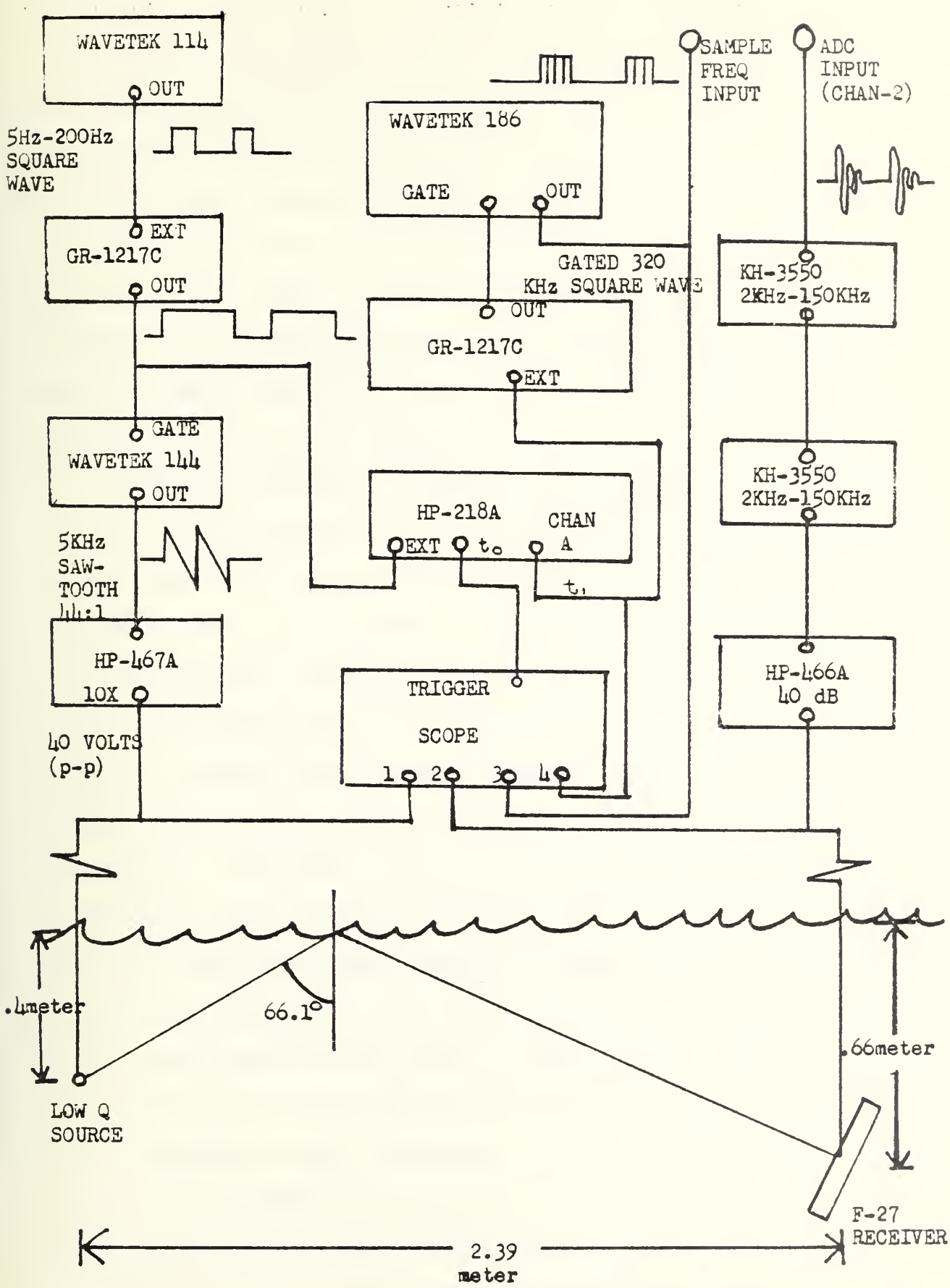

Figure 5. Experimental Setup

is composed of a sinusoid with the same fundamental as the sawtooth, as well as every harmonic of the fundamental. This signal when applied to the source was of course distorted by the frequency response of the source. Nonetheless, the fundamental and all of its harmonics were simultaneously present in the tank. It was this fact plus the gating network to be described and the FFT capabilities of the computer which permitted the analysis of 32 different frequencies at the same instant.

The gating network in figure 5 was devised to eliminate all direct path signals and those reflected from the walls of the tank. The Wavetek 114 in the upper left corner directed the entire process. The output of the Wavetek 114 was a square wave which was varied for different runs from 5 Hz to 200 Hz. It was constant during a run, however. A typical setting was 50 Hz. This produced a positive going spike every 20 msec. which triggered the GR-1217C pulse generator. The pulse out of the GR-1217C was of variable length and, when present, triggered the Wavetek 144. Thus for this example, a predetermined number of 5 kHz sawtooth cycles was emitted by the Wavetek 144 every 20 msec. This signal was amplified and sent to the source. Each positive going portion of the output of the GR-1217C also triggered the HP 218A/219 delay generator. After a preset delay, a spike was emitted by the output of the delay generator. This delay accounted for the transit time of the pulsed signal through the water. The spike from the delay generator then

triggered another GR-1217C pulse generator. The pulse out of the GR-1217C when present triggered a 320 kHz square wave pulse of variable length from the Wavetek 186.

The utility of this arrangement was that each pulse reflected from the surface could be sampled at exactly the same time relative to the initiation of the pulse. Thus a waveform reflecting off of a mirror surface should result in the identical sampled values from one run to the next. Actually there were small variations attributed to minor instabilities in the electrical apparatus. Figures 6, 7, 8 and 9 show photographs of an oscilloscope trace of sample signals. Figures 6 and 7 show the effect of the directionality of the source. The first is trained on the reflected pulse, the second on the direct path pulse. The signal received by the F-27, which was trained in the specular direction, was amplified by 40 dB and then filtered by two cascaded bandpass filters. The filter settings were chosen to eliminate 60 cycle interference and aliasing. This signal was sent to the input of the ADC.

The program that controlled the analog to digital conversion was PRKMOD. It is described in Appendix A. It avoids the problem of starting to sample in the middle of a pulse. PRKMOD is capable of recording up to 100 blocks each of 128 data points, on a cassette tape for use in further processing. This size block was always used. The block of 128 points at 320 kHz requires 0.4 msec. and the surface was assumed to be motionless in that time. This

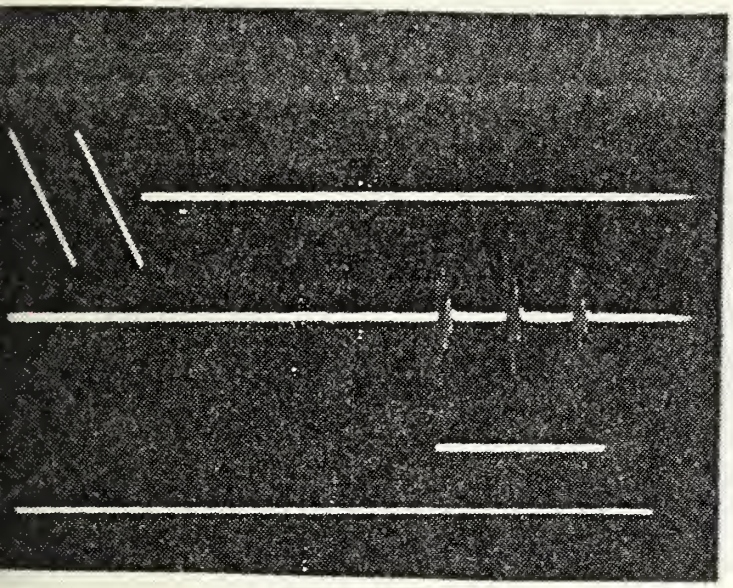

Wavetek 144 Gated 5 kHz out

Surface Reflected Sawtooth
direct path barely visible
to left of surface reflected

gated 320 kHz computer sampling
signal Wavetek 186 output

Figure 6. Analysis of Surface Reflected Pulse

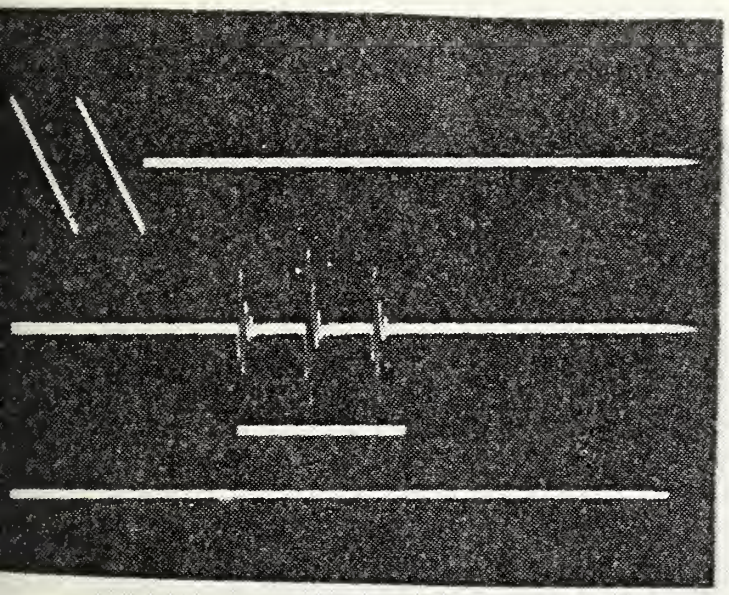

Wavetek 144 Gated 5 kHz out

Direct Path Sawtooth
surface reflected barely
visible to right of direct path

gated 320 kHz computer sampling
signal

Figure 7. Analysis of Direct Path Pulse

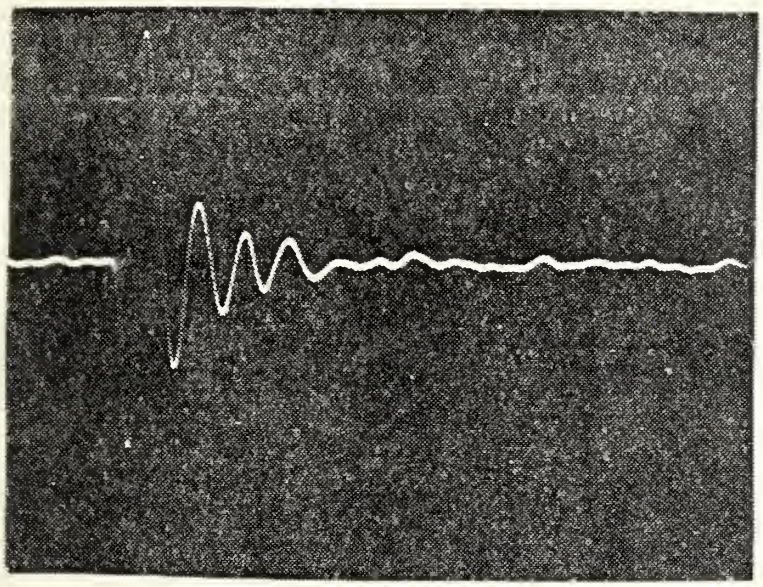

Expanded single pulse out of LOWQ point source. This demonstrates the ringing of the source.

Figure 8. Source "Ringing"

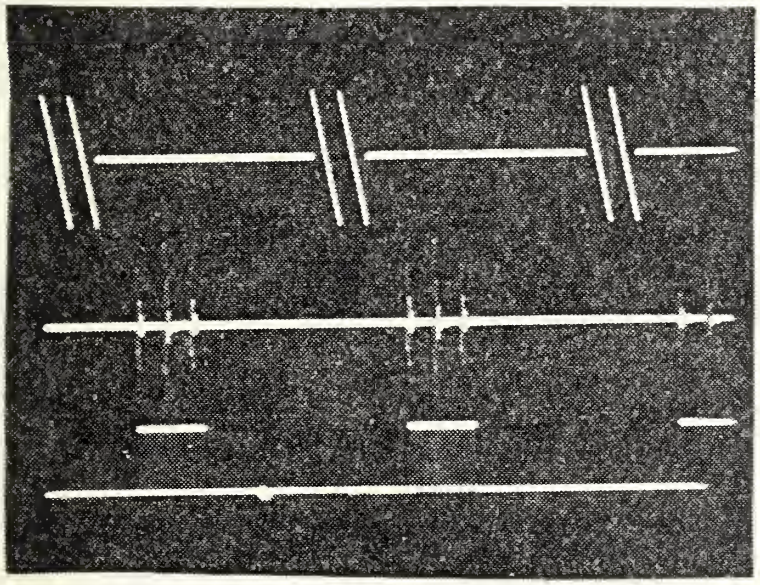

Series of pulses shown with a 20 msec separation.

Figure 9. Series of Pulses and Reflections

is a good assumption as previous tank studies have shown that the wave height spectral density is down by a factor of 1000 from its peak and is continuing to drop at the rate of $f^{-5.5}$ at 10 Hz. This indicates that there is negligible change of surface height in 0.4 msec. With a 50 Hz pulse repetition rate for the entire system, 100 data blocks thus translates into 2 seconds of real time. Another standard pulse repetition rate was 16.7 Hz, 100 blocks here translates into 6 seconds of real time.

It is important to remember that this experiment attempted to model the real ocean. Loomis and Perkins showed typical energy peaks of the wave height spectrums in the model tank to be approximately 2.5 Hz. This corresponds for example to a peak spectral density at 0.1 Hz for a Pierson-Moskowitz sea with a wind speed of 14 m/sec (approximately 28 knots). Thus 2 seconds of real time in the wave tank might contain 5 wave periods. Five wave periods at sea would consume about 50 seconds of "ocean time". Similarly, 6 seconds in the wave tank would encompass about 15 wave periods and would translate into 150 seconds of "ocean time". The point is that these short times in the wave tank correspond to significant time periods in the real world.

Thus the output of PRKMOD was a digital cassette of 100 blocks, each containing 128 sampled values. This tape would be input to THCDB2, described in appendix A. This program performed an FFT on each block of 128 points. The available frequency resolution, assuming a sampling frequency of 320 kHz,

was 2500 Hz. The result of each FFT, however, was output on a digital cassette in 5 kHz steps. This output was an amplitude in dB and its phase in radians for the particular frequency. The program calculated the average amplitude in dB, the standard deviation in dB, the mean phase in radians and the standard deviation in radians. The output of a typical direct path run is provided in table I.

C. ELECTRICAL AND MECHANICAL STABILITY ANALYSIS

Loomis (Ref. 8) encountered problems with the mechanical stability of his apparatus under conditions of high wind speed and the ensuing large wave height. This problem was solved in this research by attaching the mounts of the receiver and source together and securing each of these firmly to the sides of the tank with thin copper wire. Though this wire did lie in the path of the sound, it was very much smaller than a wavelength of even the highest frequency (160 kHz) and thus did not significantly disturb the pressure measured at the receiver.

Loomis also encountered increasing instability with frequency from one pulse to the next in direct path analysis and analysis of the sound reflected from a mirror surface. This showed up in a fairly large standard deviation in amplitude at the higher frequencies. Referring to figure 5, instead of the pulse generator in the sampling circuit which gates the 320 kHz square wave, he used a tone burst generator to pass the sampling signal. The problem there was that

FREQ (Hz)	Mean Amplitude (dB)	Std. Dev. Amplitude (dB)	Mean Phase (radians)	Std. Dev. Phase (radians)
0.0	-44.839	-61.360	0.000	0.000
5000.0	-45.399	-62.561	2.659	0.137
10000.0	-26.984	-66.417	1.499	0.025
15000.0	-23.877	-63.183	1.266	0.012
20000.0	-22.872	-63.183	1.164	0.007
25000.0	-22.616	-65.257	1.447	0.007
30000.0	-19.704	-63.954	1.445	0.004
35000.0	-18.066	-63.319	1.381	0.004
40000.0	-16.155	-64.794	1.482	0.005
45000.0	-13.431	-68.378	1.375	0.006
50000.0	-11.027	-65.257	1.208	0.008
55000.0	-8.727	-60.786	0.972	0.010
60000.0	-7.125	-57.196	0.563	0.012
65000.0	-8.017	-60.206	0.133	0.013
70000.0	-8.090	-59.943	-0.250	0.014
75000.0	-10.195	-72.247	-0.684	0.015
80000.0	-12.879	-75.000	-0.937	0.015
85000.0	-14.998	-69.517	-1.184	0.014
90000.0	-16.996	-64.245	-1.387	0.013
95000.0	-17.697	-65.257	-1.782	0.012
100000.0	-20.006	-66.807	-2.463	0.008
105000.0	-24.241	-60.160	3.113	0.005
110000.0	-28.965	-57.754	2.229	0.024
115000.0	-34.307	-61.262	1.287	0.074
120000.0	-37.597	-67.236	0.060	0.121
125000.0	-37.419	-57.641	-1.312	0.028
130000.0	-38.671	-61.484	-2.201	0.063
135000.0	-39.019	-63.580	-2.433	0.069
140000.0	-37.189	-64.856	-2.492	0.040
145000.0	-35.370	-64.791	-2.637	0.018
150000.0	-34.031	-66.286	-2.804	0.018
155000.0	-33.391	-67.811	-2.977	0.010
160000.0	-33.489	-67.835	3.142	0000.000

TABLE I

the tone burst would not always start with an upgoing pulse. It would start at any point in the cycle. At lower frequencies this would not make much difference, but at the higher frequencies this instability became quite serious. The pulse generator used in this research solved this by always starting the sampling burst on an upgoing pulse.

These two modifications brought about excellent run-to-run stability throughout the entire bandwidth as shown in table I. This was a 50 block run, analyzing the direct path signal, with 5 fans turned on, which was the situation of maximum RMS waveheight. The phase stability is excellent, the standard deviation is on the order of 0.02 radians or about 1°. The amplitude standard deviation is normally 40 dB below the mean amplitude. The result of runs analyzing the signal reflected off of a mirror surface was very similar to that of table 1. The value at 160 kHz was always suspect in these runs as it generally had a mean phase of 0 or π radians. Thus only frequencies from 5 kHz to 155 kHz were analyzed. This gave a total of 31 simultaneous frequencies available for analysis. Runs were made under a variety of fan combinations and at angles of incidence of 24.3°, 66.1°, 44.1", 32.6°, and 45.9". Several different pulse repetition rates were attempted from 5 Hz to 200 Hz. Going below 16.7 Hz gave very spotty coverage especially at the higher frequencies and going above 50 Hz gave too short a time for much analysis. Thus these two pulse repetition rates were used exclusively. As shown above, at an ocean

wind speed of 14 m/sec the 50 Hz rate corresponds to about 5 ocean periods and about 50 seconds of "ocean time"; 16.7 Hz corresponds to about 15 ocean wave periods or 150 seconds of "ocean time".

V. EXPERIMENTAL RESULTS AND ANALYSIS

A. INITIAL LOOK AT SPECULARLY SCATTERED SOUND

The output of THCDB2 had up to 100 FFT,s each with a 5 kHz resolution. This was read out on a digital cassette and this is where the processing began. SORTPLOT, which is described in Appendix A, plots the amplitude in dB vs. time for each frequency. Figure 10 is an example of the output of SORTPLOT. Each individual plot is a record of how the surface reflected pressure varied during this 2 second run. This run was taken using the rough surface caused by one fan and at the angle of incidence 66.1°. Because of the low RMS waveheight with one fan and the large angle of incidence, there was a low roughness parameter g even for the highest frequencies in this run. Even with such a relatively smooth surface, there are variations on the order of 30 dB in the upper frequencies. Loomis (Ref. 8) shows that the peak of the wave height spectrum for one fan is approximately 3.3 Hz in the tank. Notice that most of the lower frequencies have 6 or 7 periods over this two second run. This points out the fact that the lower frequencies only pick up the larger scale variations in the water surface. The higher frequencies are much more ragged as they respond to the very small scale variations in surface height. For a greater surface roughness or a smaller angle of incidence, g increases. When runs like these were attempted, the large scale variations occurred at much lower frequencies.

FIGURE 10

Simultaneous pressure amplitude vs. time for each of 31 frequencies. The first number below the graph is the frequency and the second is the dynamic range of the frequency for the run. The solid line is the mean of the frequency for the run. The dashed line is 3 dB below the mean. Note the different scales for each frequency. The angle of incidence is 66.1°. It is a 1 fan surface.

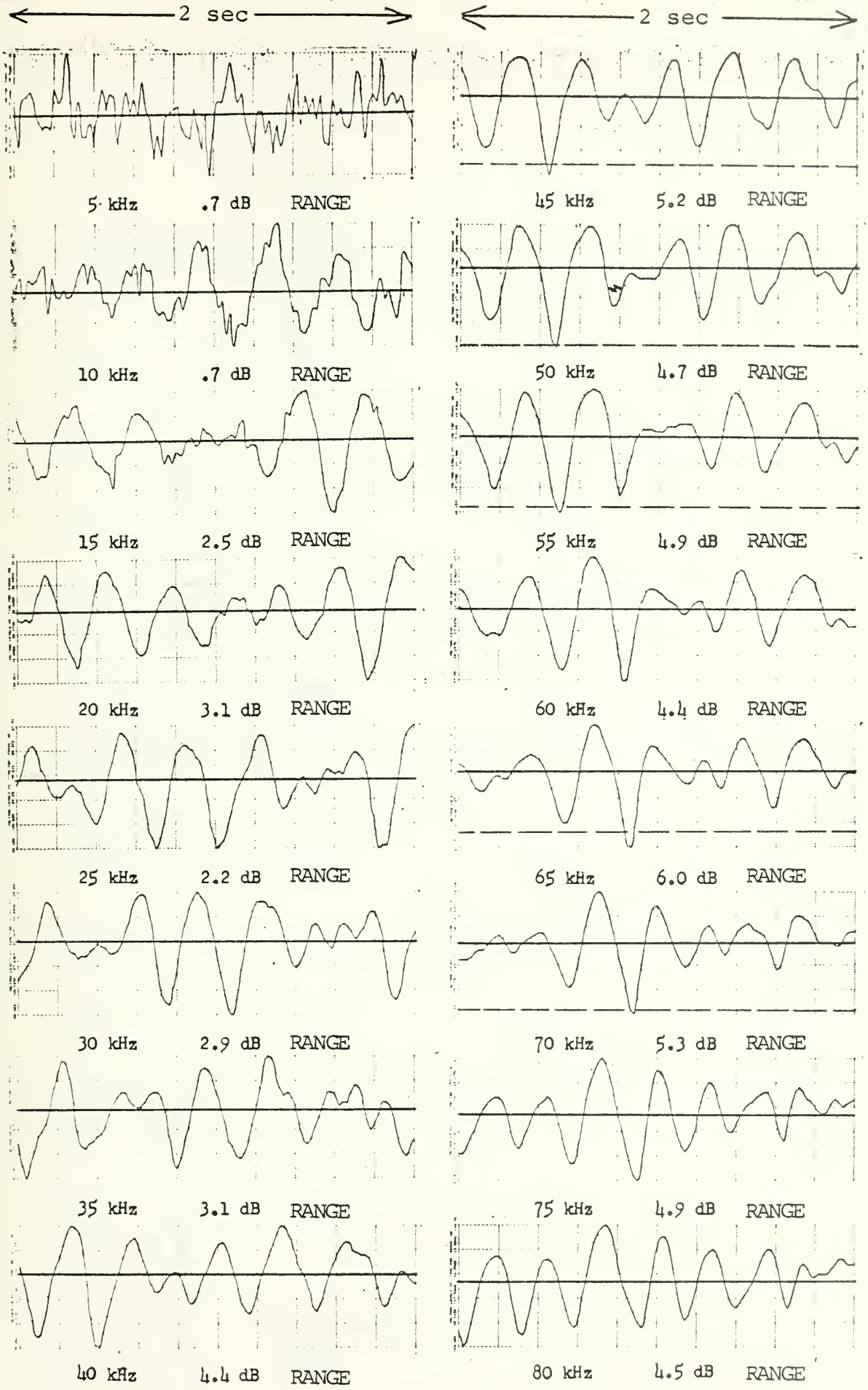
2 sec
2 sec
5 kHz .7 dB RANGE
45 kHz 5.2 dB RANGE
10 kHz .7 dB RANGE
50 kHz 4.7 dB RANGE
15 kHz 2.5 dB RANGE
55 kHz 4.9 dB RANGE
20 kHz 3.1 dB RANGE
60 kHz 4.4 dB RANGE
25 kHz 2.2 dB RANGE
65 kHz 6.0 dB RANGE
30 kHz 2.9 dB RANGE
70 kHz 5.3 dB RANGE
35 kHz 3.1 dB RANGE
75 kHz 4.9 dB RANGE
40 kHz 4.4 dB RANGE
80 kHz 4.5 dB RANGE

Figure 10

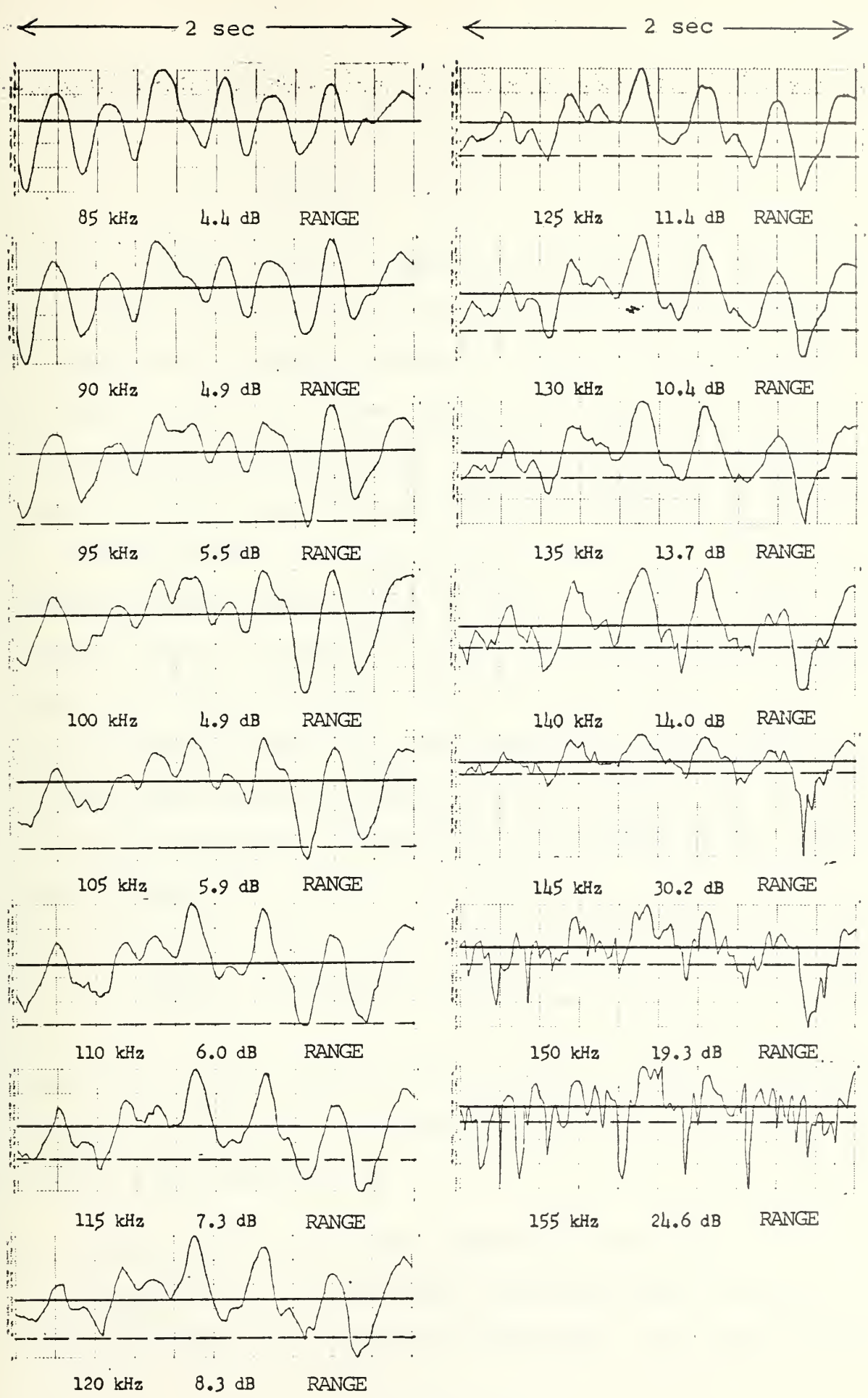
2 sec
2 sec
85 kHz 4.4 dB RANGE
125 kHz 11.4 dB RANGE
90 kHz 4.9 dB RANGE
130 kHz 10.4 dB RANGE
95 kHz 5.5 dB RANGE
135 kHz 13.7 dB RANGE
100 kHz 4.9 dB RANGE
140 kHz 14.0 dB RANGE
105 kHz 5.9 dB RANGE
145 kHz 30.2 dB RANGE
110 kHz 6.0 dB RANGE
150 kHz 19.3 dB RANGE
115 kHz 7.3 dB RANGE
155 kHz 24.6 dB RANGE
120 kHz 8.3 dB RANGE

Figure 10

Table II shows the averages and standard deviations of the surface reflected pressures of a 2 second run at a smaller angle of incidence, 32.6°, but still with a 1 fan surface. Though table I showed the results for a direct path signal these two tables can still be compared keeping in mind that the mirror reflected results were very similar to those of table I. Thus comparing the two, it is immediately obvious that the phase standard deviation is much larger for the rough surface reflected situation. Also for this situation the phase standard deviation climbs gradually until about 70 kHz and then it shoots up very rapidly until at 95 kHz and beyond the phase appears to be spread out very uniformly. This will be looked at in greater detail later. Also the average amplitude falls off much more rapidly in table II than in table I with increasing frequency. This is not surprising as the theory predicts that for a Gaussian surface

$$\frac{\langle p \rangle}{p_o} = \exp(-g/2) \ .$$

This says that the ratio of the average reflected pressure divided by the mirror reflected pressure will fall off sharply with increasing g.

B. EXAMINATION OF PHASE AND AMPLITUDE VARIATIONS

HISTOGRAM is a program that provides phase and amplitude histograms for a specified bandwidth. An output of up

FREQ (Hz)	Mean Amplitude (dB)	Std. Dev. Amplitude (dB)	Mean Phase (radians)	Std. Dev. Phase (radians)
0.0	-38.564	-57.979	3.142	0.012
5000.0	-46.251	-65.886	-0.884	0.168
10000.0	-33.561	-58.008	-1.653	0.040
15000.0	-31.102	-53.333	-1.928	0.097
20000.0	-30.877	-49.621	-2.035	0.100
25000.0	-30.679	-51.832	-1.929	0.155
30000.0	-28.037	-43.954	-1.820	0.175
35000.0	-25.841	-38.685	-1.933	0.183
40000.0	-24.560	-36.517	-2.000	0.217
45000.0	-21.562	-32.528	4.246	0.261
50000.0	-19.087	-28.762	3.985	0.286
55000.0	-17.602	-26.425	3.565	0.312
60000.0	-16.882	-24.808	3.104	0.398
65000.0	-18.470	-25.152	2.558	0.527
70000.0	-19.374	-25.162	2.091	0.641
75000.0	-22.834	-27.884	1.942	1.195
80000.0	-25.968	-30.552	1.841	1.238
85000.0	-28.488	-32.603	1.896	1.535
90000.0	-30.571	-34.595	1.957	1.662
95000.0	-31.150	-35.421	2.270	1.984
100000.0	-33.109	-37.666	3.004	2.239
105000.0	-37.334	-41.876	3.478	2.234
110000.0	-43.374	-47.381	4.090	2.131
115000.0	-45.300	-49.587	3.621	2.351
120000.0	-43.249	-48.034	3.453	2.265
125000.0	-41.982	-46.797	3.566	2.124
130000.0	-44.427	-48.526	3.688	2.067
135000.0	-48.821	-53.677	3.415	2.207
140000.0	-51.565	-56.322	3.676	2.411
145000.0	-53.488	-57.873	3.667	2.600
150000.0	-53.753	-57.868	4.337	2.465
155000.0	-53.860	-58.778	3.284	2.878
160000.0	-53.808	-58.331	0.110	0.556

TABLE II

to 100 FFT's from THCDB2 is used as the input for this program. The reflection of sound off of a rough surface can be described as passing sound through a channel that adds some noise. Reference 9, chapter 4 provides the theoretical description for this problem. Looking just at phase variation, theory predicts that the phase shift of sound reflected off of a mirror surface is constant. Its PDF would be a delta function. As the surface becomes rougher, the distribution shifts gradually to uniform. Figures 11, 12, and 13 illustrate this process nicely, they are phase histograms for 15 kHz, 40 kHz and 125 kHz respectively, with a 1 fan rough surface. The distribution changes from a very sharp spike to practically a uniform distribution.

As for amplitude variation, in the low roughness situation, the distribution should be roughly Gaussian but with a non-zero mean. As the surface becomes rougher or the signal to noise ratio decreases, the mean of the distribution approaches zero. However it never reaches zero. In the very rough case, it approaches a Rayleigh distribution. This theory is borne out in figures 14, 15 and 16. With increasing g, the distribution changes from approximately Gaussian to approximately Rayleigh.

C. SEPARATION OF THE COHERENT COMPONENT

As described in the introduction, Loomis, after visual study of graphs similar to those of figure 10, postulated that there was a constant frequency separation or delta

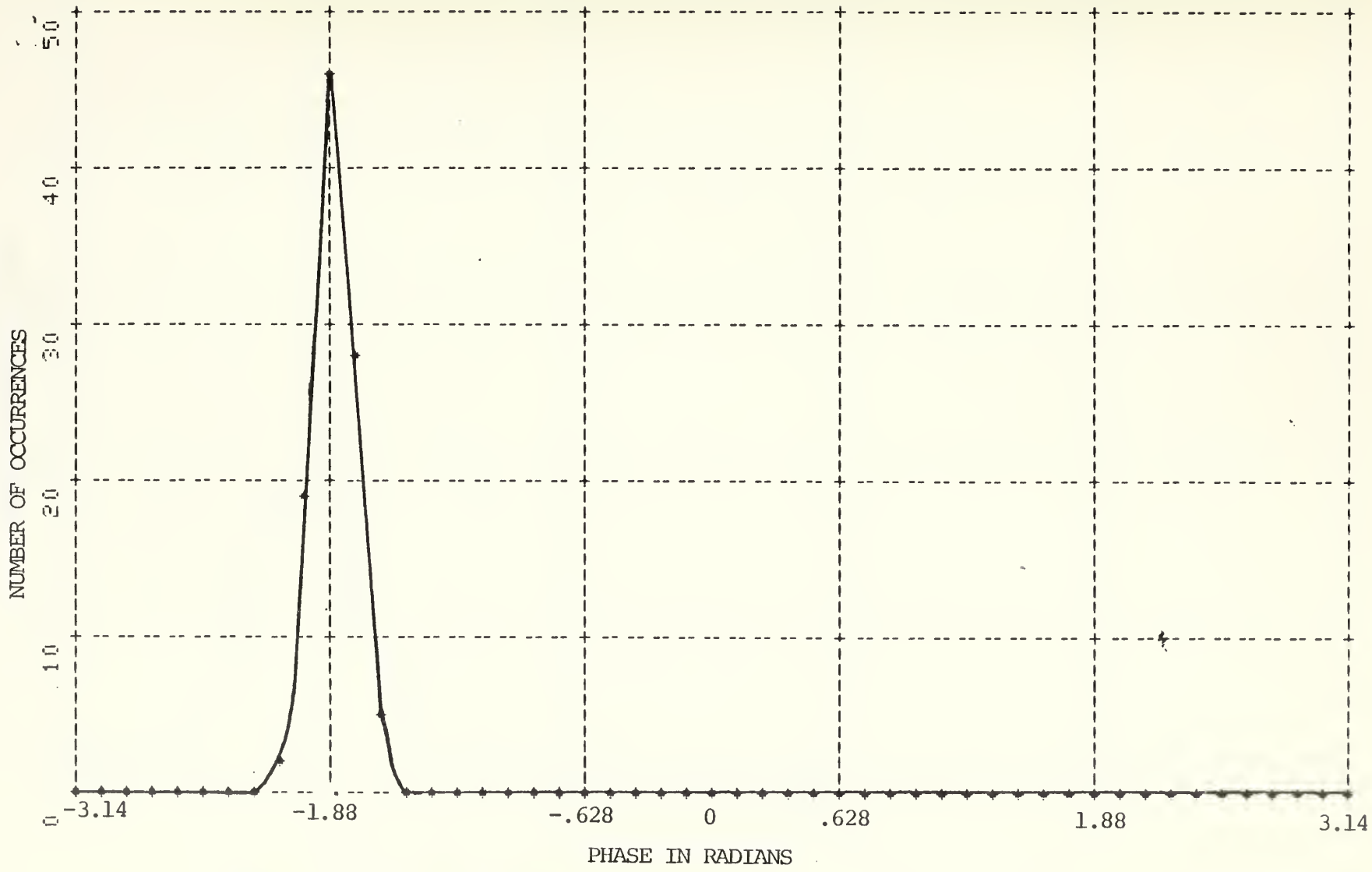

Figure 11. Phase Histogram at 15 kHz. 1 Fan Sea.

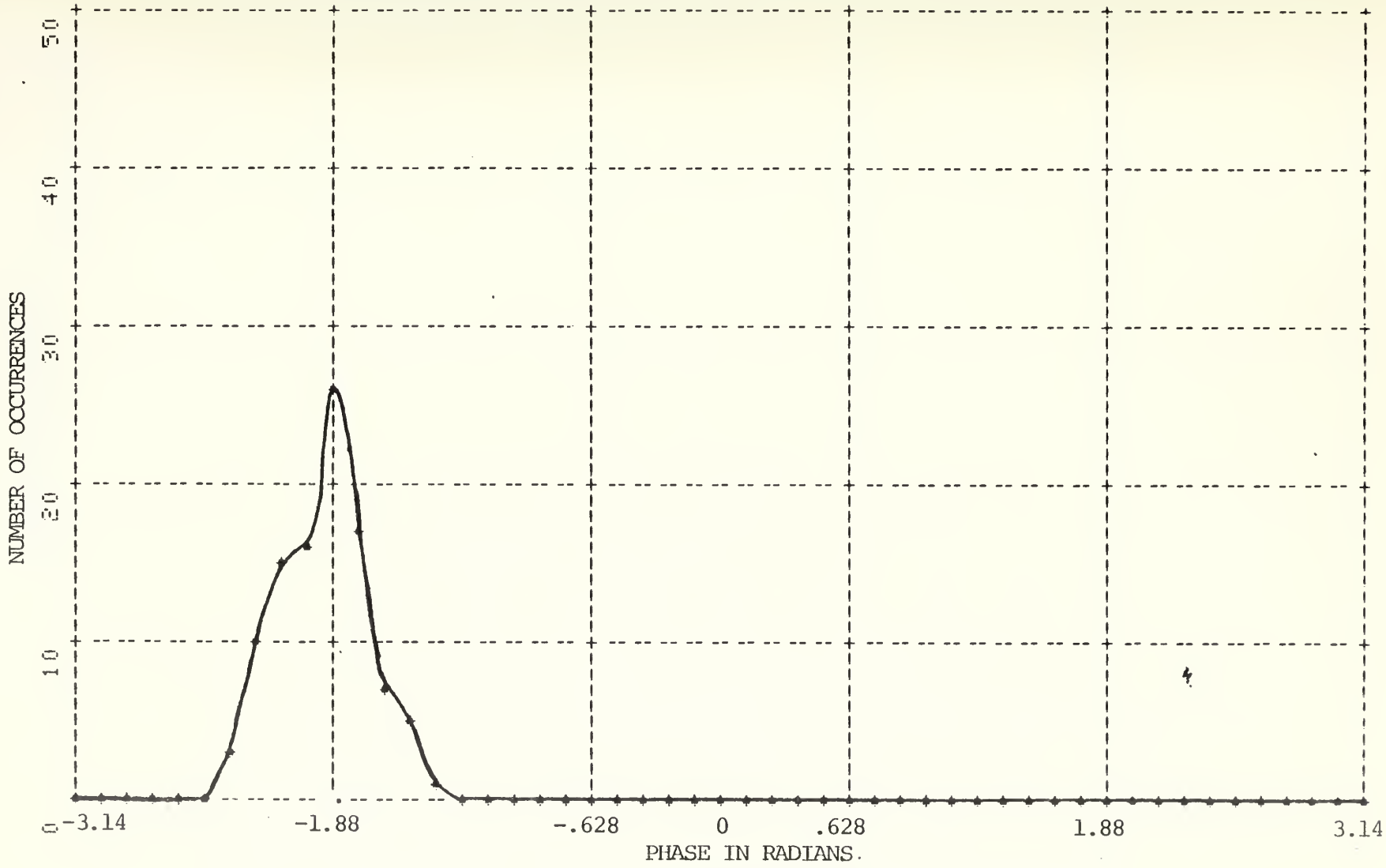

Figure 12. Phase Histogram at 40 kHz. 1 Fan Sea.

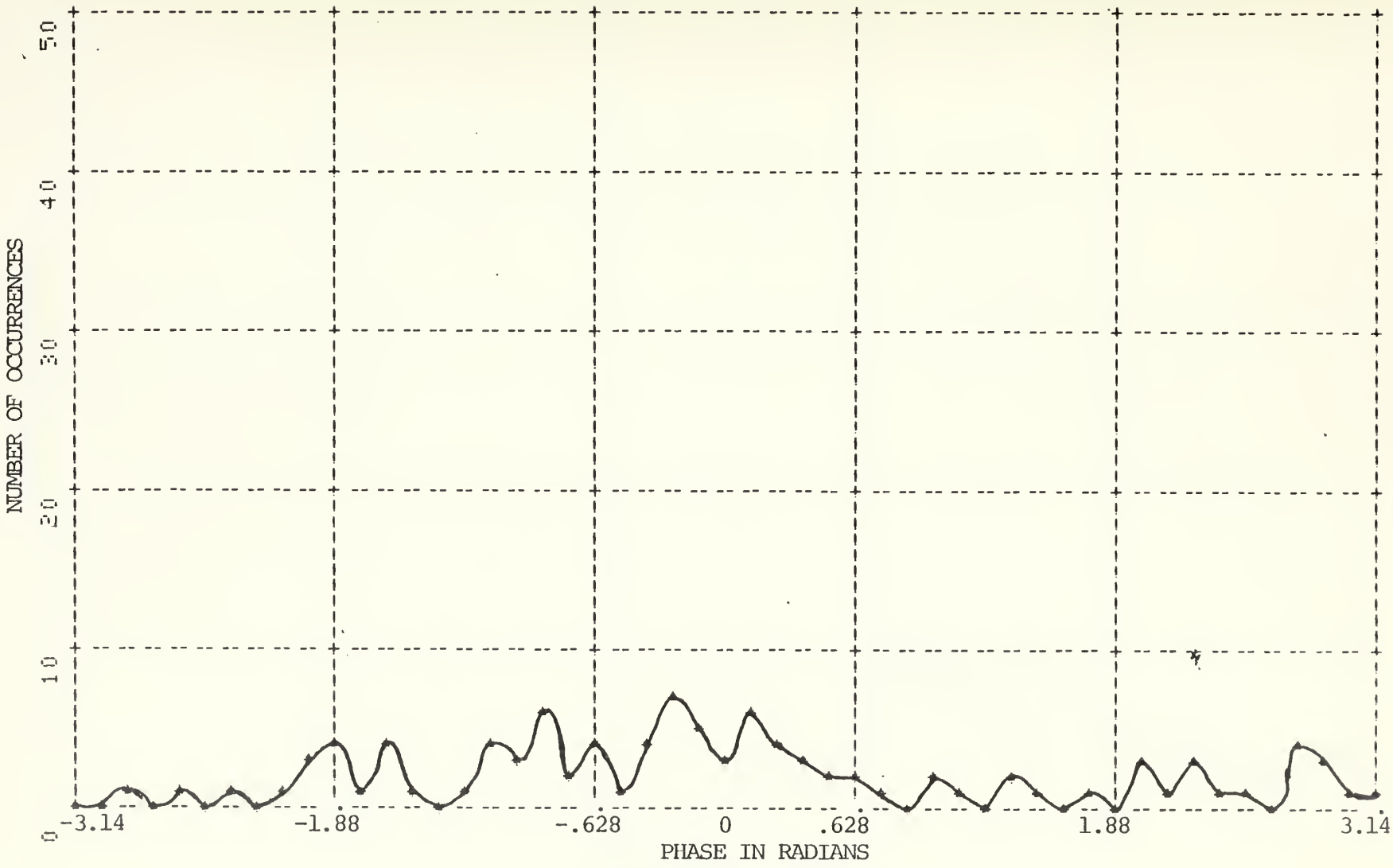

Figure 13. Phase Histogram at 125 kHz. 1 Fan Sea.

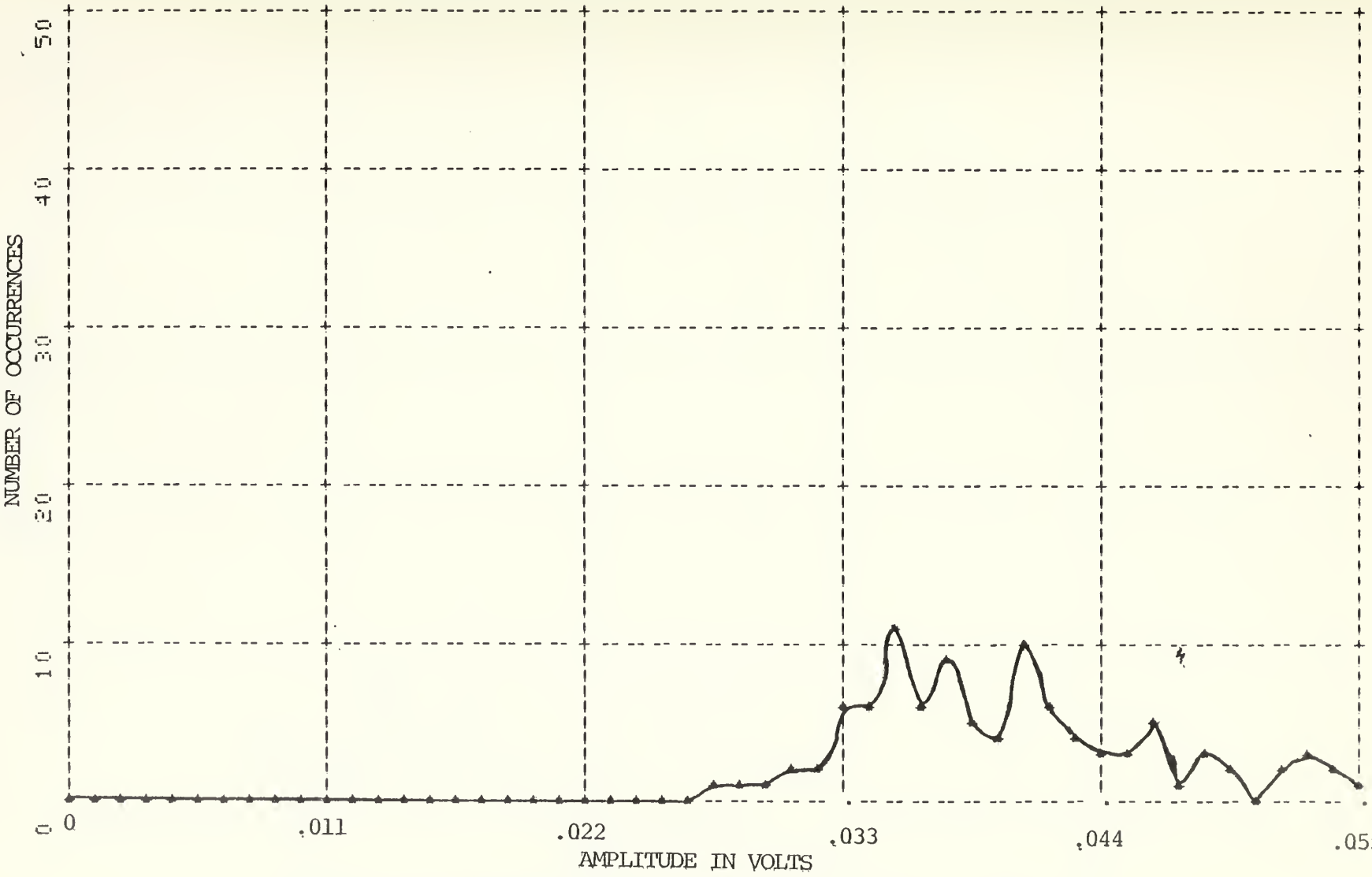

Figure 14. Amplitude Histogram at 30 kHz. 1 Fan Seq.

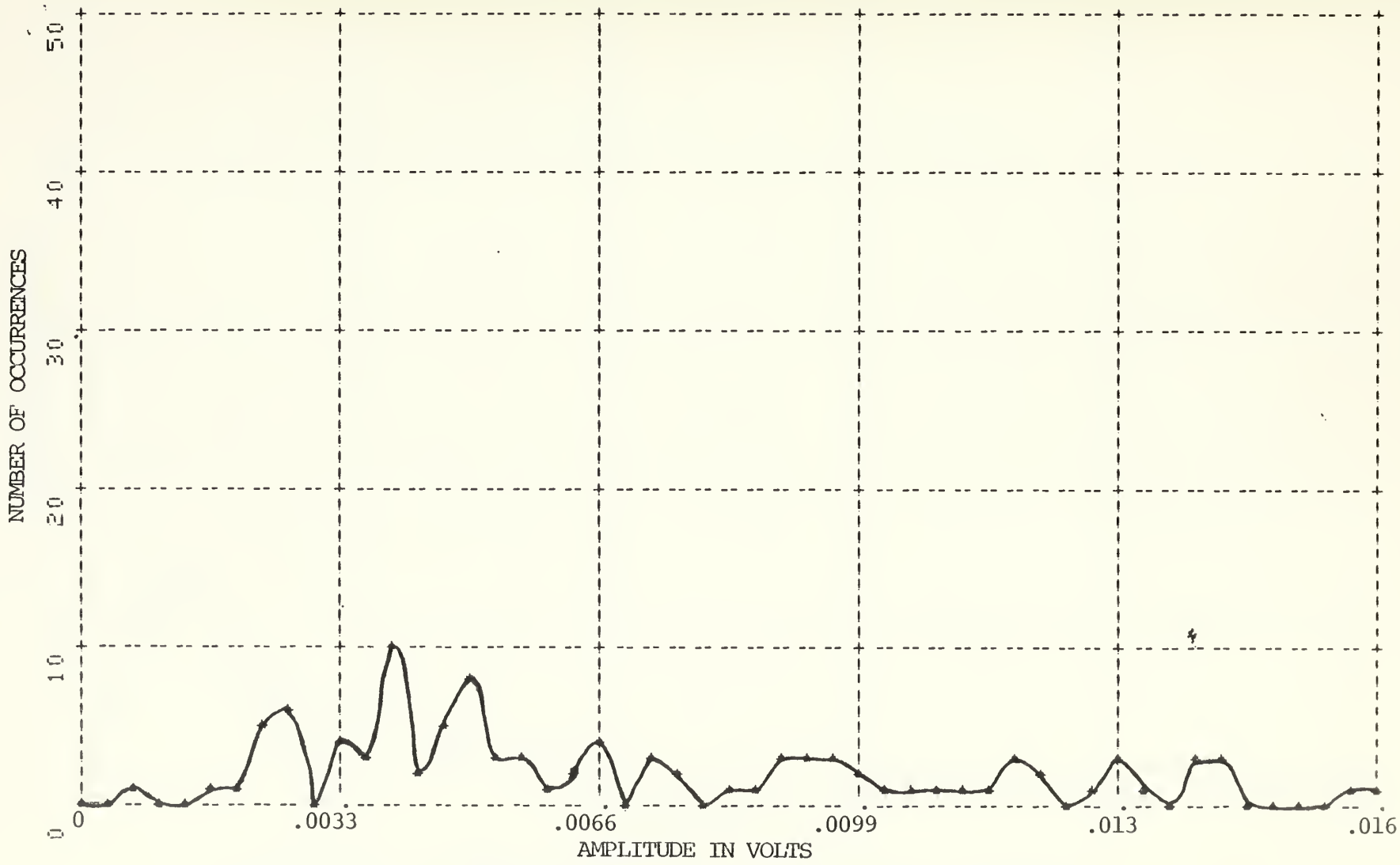

Figure 15. Amplitude Histogram at 120 kHz. 1 Fan Sea

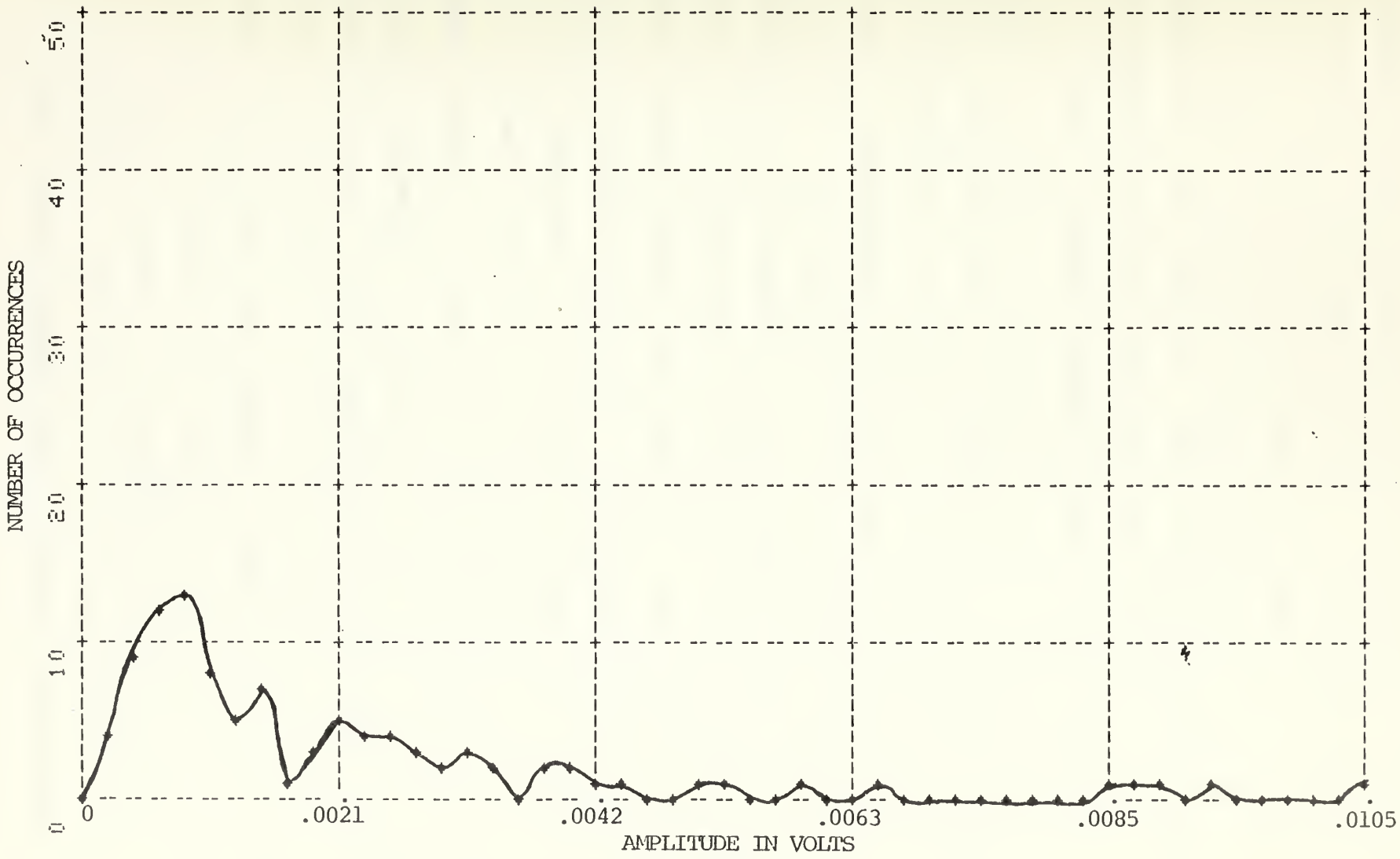

Figure 16. Amplitude Histogram at 155 kHz. 1 Fan Sea.

frequency between amplitude maxima and minima at any instant of time for a given RMS waveheight. Furthermore, he felt that the effect would be strongest for small g. He predicted the coherent component at higher roughnesses would also display the same behavior. Thus it was desirable to separate the coherent component from the total pressure.

Figure 17a shows a phasor diagram of the reflected signal received at any instant of time. The surface is fairly rough and there is a significant incoherent component. Each amplitude A_j at phase ϕ_j is reflected off of a horizontal facet in the surface as the receiver is in the specular direction. The resultant $re^{i\psi}$ is the actual complex pressure detected by the receiver at this instant. The signal was previously measured after reflection off of a mirror surface, otherwise the geometry was identical. This signal was totally coherent and was $\bar{r}e^{i\bar{\psi}}$. The utility of this approach is that thereafter at any instant of time, the component of any successive resultant in the direction of $\bar{\psi}$ can be determined as in figure 17b. This will be defined as the coherent component. FREQCO MOD 3, which will be more fully described later, has the capability of transforming all data values in this manner if the mirror surface values of phase are read into the computer. THCDB2 also attempts this process, if requested, but instead of using the mirror surface values of phase, it calculates an average phase for each frequency. This should be a good appproximation but in a fairly uniform distribution of phase, the technique

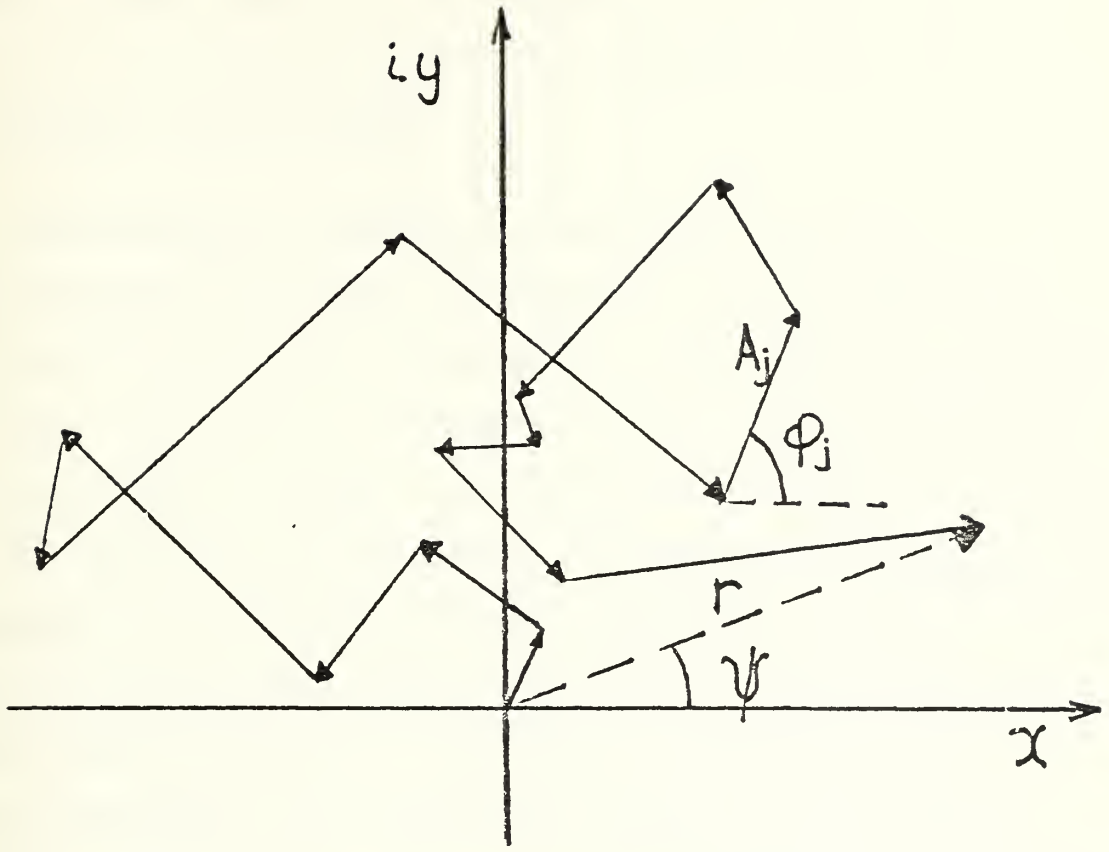

Figure 17a. Instantaneous Received Signal

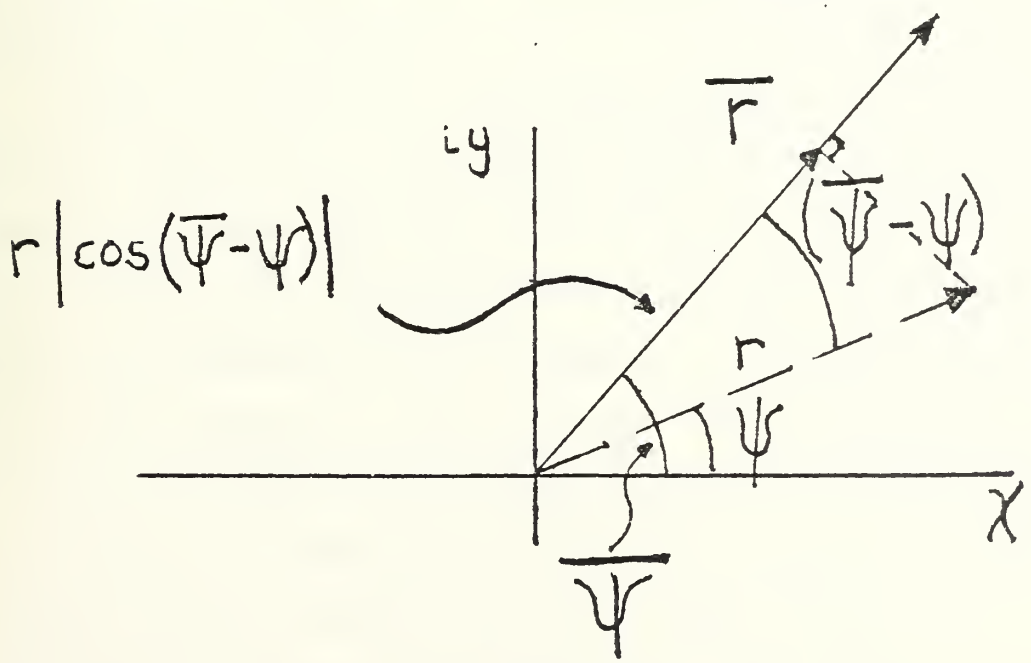

Figure 17b. Coherent Component

used to avoid the π, $-\pi$ discontinuity breaks down and a proper average cannot be calculated. Thus THCDB2 can be used for low roughness situations where the phase is distributed fairly tightly.

D. INTERFREQUENCY CORRELATION VS. DELTA FREQUENCY

Examining the minima of figure 10, it is possible to see patterns emerging as one shifts from one frequency to the next. By laying a straightedge along an identifiable minimum in each frequency one generates a slope. This slope is what gave rise to the idea of a change from a maximum to a minimum in a certain frequency separation or delta frequency. The difficulty here is that the slope is not constant from one section of the graph to another. Also minima disappear and sometimes reappear as one tries to follow a minimum through several frequencies. This was the technique used by Loomis.

It was decided that a computer analysis of all of the data was required, as this would not be affected by subjective judgments of maxima and minima. A computer algorithm which finds the interfrequency correlation vs. delta frequency was developed (SON OF FREQCO); it examined fluctuations about each frequency's mean in the following manner.

First, as there was approximately a 35 dB spread in the source-receiver combination between the maximum average pressure and the minimum, as can be seen in table II, a normalization routine was called for. This routine gave

each frequency an identical mean pressure. It amplified each value, for each frequency, by the ratio of the maximum average pressure to that of its own average pressure. This procedure took out the frequency dependence of the source and receiver but also eliminated the $e^{-g/2}$ dependence of the amplitude on the surface roughness. Continuing:

$$\Delta p = p_i - \langle p_i \rangle = [\text{Instantaneous pressure}] - [\text{Average pressure}].$$

For N frequencies, there are N (Δf)'s from $\Delta f = 0$ to $\Delta f = N-1$. As an example of this if one had 25 harmonic frequencies say from 5 kHz to 125 kHz, there would be 25 (Δf)'s ranging from 0 to 120 kHz. There would be 25 pairs of frequencies with a $\Delta f = 0$, 24 pairs with a $\Delta f = 5$ kHz and so on until there was one pair with a $\Delta f = 120$ kHz (5 kHz and 125 kHz).

Therefore, SON OF FREQCO, for each time step, calculates:

$$\left[\frac{1}{\dfrac{\sum_{n=1}^{N} (\Delta p_n)^2}{N+1}} \right] \frac{\sum_{n=1}^{N-a} (\Delta p_n)(\Delta p_{n+a})}{N + 1 - a}$$

where $a = \Delta f/5$ kHz and $0 < a < N-1$. The expression in the brackets is simply the expression on the right where a or $\Delta f = 0$, it is a normalization factor which causes the value at $\Delta f = 0$ to be 1. The expression at the right is simply the average of the pressure fluctuations at one

frequency times those of another at a certain Δf. Notice that the sign is maintained in this operation. This is important because a negative sign indicates that the average fluctuations about the mean for a particular Δf are out of phase at this time step. At this point there are N average correlations corresponding to the N (Δf)'s for each time step. The final step is to average these N correlations over all of the time steps and then plot the correlation vs. Δf.

Runs were taken using all fan combinations with the setup of figure 5, but with an angle of incidence of 32.6°. These runs were analyzed with the aid of SON OF FREQCO. This program also has the ability to make computations over any bandwidth for any number of time steps. Figures 18 and 19 were selected from approximately 100 computer runs to demonstrate the results of this analysis. What had been expected to confirm Loomis' results was a strong negative correlation at a certain delta frequency which would be consistent over a considerable length of time. Figure 18, however, was typical of most of the runs that carried on for any signficant amount of time. The correlation exhibits an exponential decay as the frequency separation increases until at approximately 80 kHz the correlation is zero. This run was analyzed over its full length of 2.0 seconds. Needless to say, these results were disappointing and did not support Loomis' conclusions. On the other hand, they were supportive of the conclusions of Ref. 5.

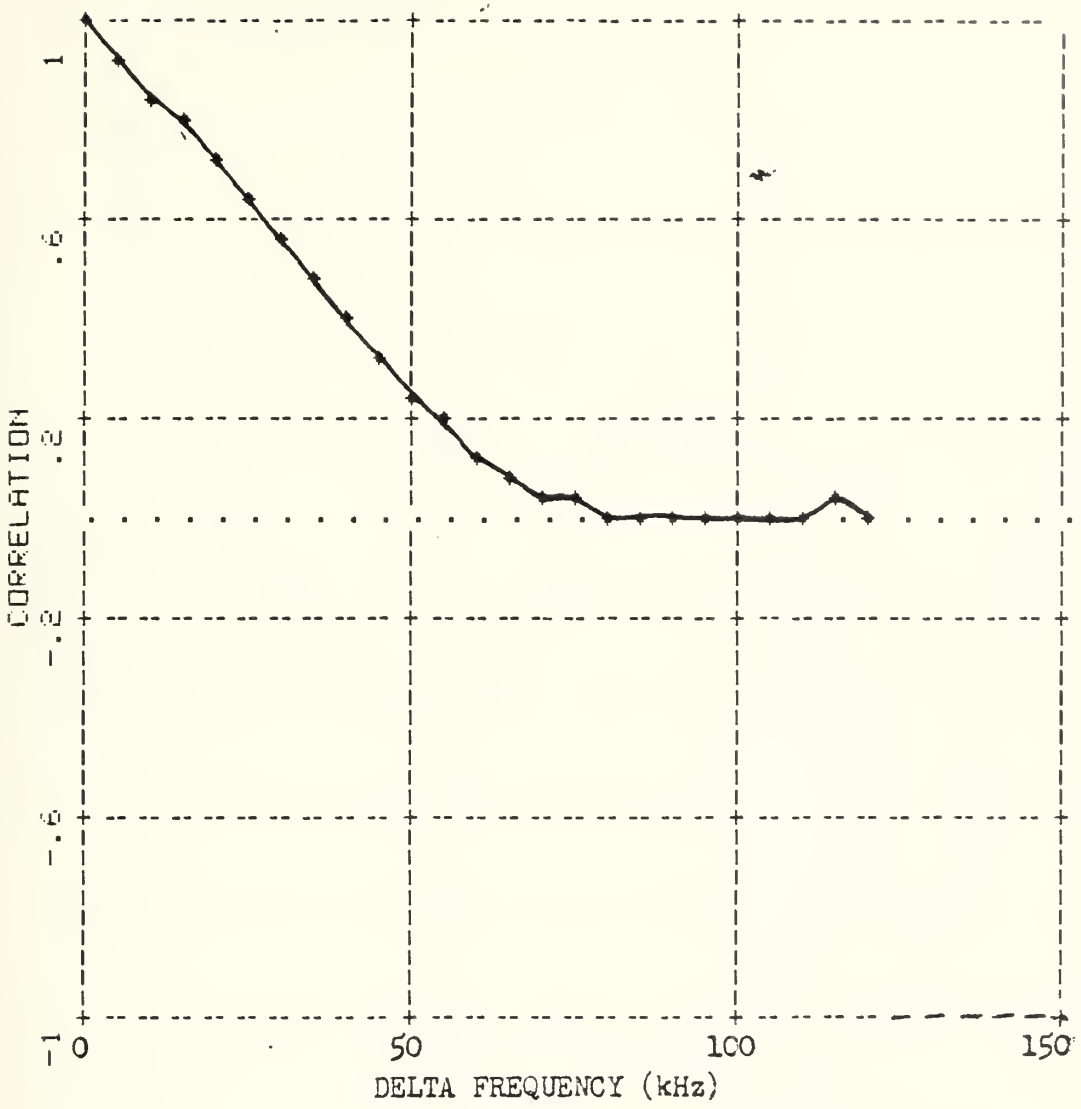

Figure 18. Interfrequency Correlation vs. Delta Frequency

1 Fan at angle of incidence 32.6°
Correlation taken of 25 frequencies over 2.0 seconds

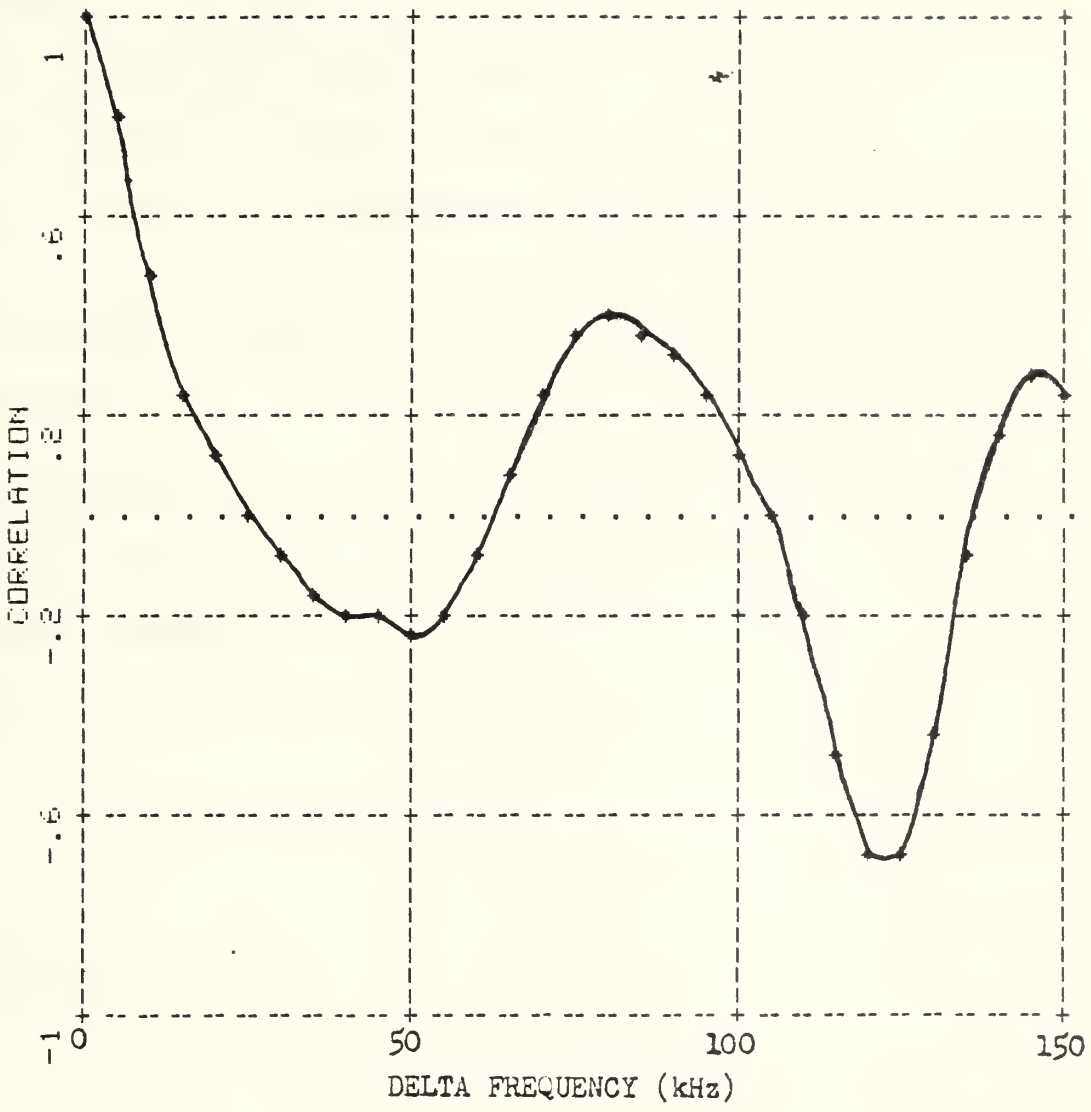

Figure 19. Interfrequency Correlation vs. Delta Frequency

3 Fans at angle of incidence 32.6°
Correlation taken of 31 frequencies over 160 msec.

Interesting results could be obtained by restricting the time interval to very short periods. Figure 19 is an example of a computer run taken over only 8 time steps or 160 msec. This graph shows dramatic negative correlations, but when averaged over any significant time period the peaks and troughs of figure 19 smooth out to something like those of figure 18. A new approach was needed. The theory of specular scatter was then reconsidered to determine under what conditions a maximum or minimum could be produced by interferences.

E. INTERFREQUENCY COVARIANCE VS. FREQUENCY RATIO

For the sinusoidal surface of figure 20, the path difference between the two rays, which are specularly scattered from horizontal facets, is:

$$\Delta r = 2\, h \cos \theta .$$

The phase difference is

$$\Delta \phi = \frac{4\pi h}{\lambda} \cos \theta$$

as shown in the theory section. Now as the RMS waveheight σ is known in terms of h for a sinusoidal surface, $\sigma = \frac{h}{2\sqrt{2}}$ we find:

$$\Delta \phi = \frac{2\sqrt{2} \times 4\pi\sigma}{\lambda} \cos \theta = 2\sqrt{2}(g)^{\frac{1}{2}} .$$

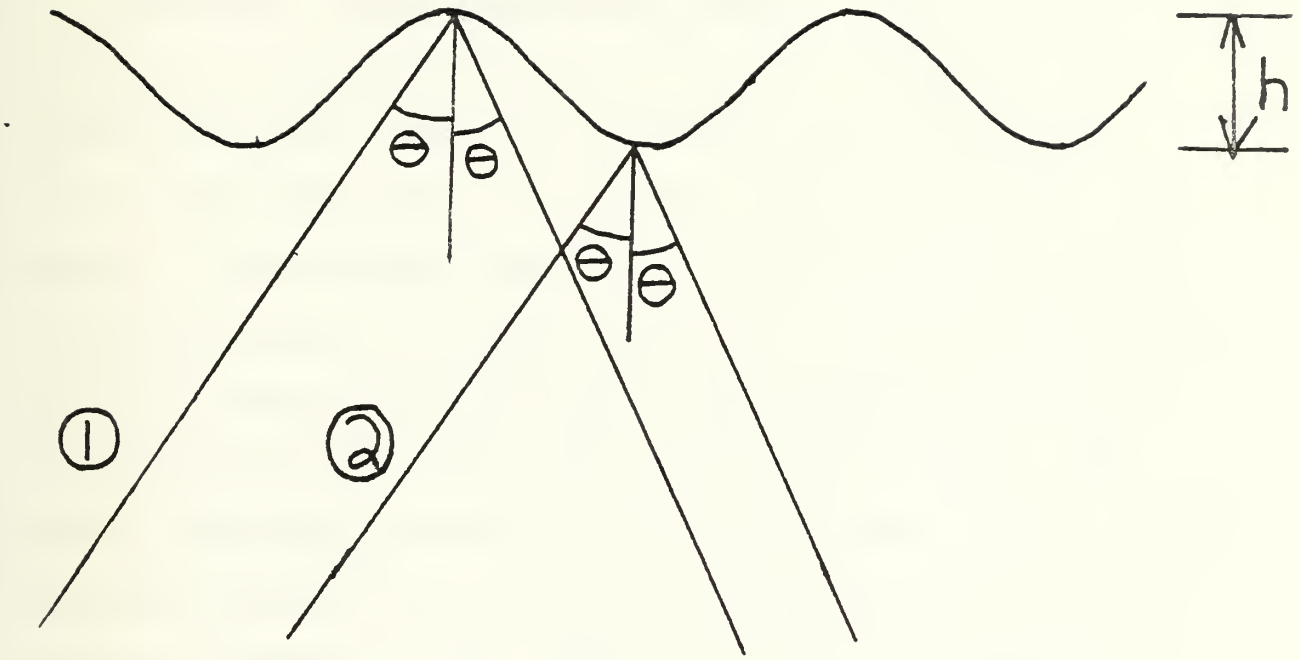

Figure 20. Specular Reflection from a Sinusoidal Surface

For complete interference $\Delta\phi = \pi$ and thus

$$\pi = 2\sqrt{2}(g)^{\frac{1}{2}}$$

solving for $(g)^{\frac{1}{2}}$ one obtains: $(g)^{\frac{1}{2}} = 1.11$ for an amplitude minimum.

Therefore, <u>for a sinusoidal surface</u>, complete cancellation could be expected when $(g)^{\frac{1}{2}} = 1.11$. Another way of looking at this situation is that the path difference is $\lambda/2$ at this frequency of interest. Now if the second harmonic of this primary frequency were also present, the path difference would be a full wavelength for the second harmonic. In this case the second harmonic experiences constructive interference and an amplitude maximum would occur. This case is certainly oversimplified as the near Gaussian surface has been modeled by a sinusoid of the frequency of maximum spectral density. Also, especially at higher frequencies, the reflection is much more complex than shown by the two rays in figure 20. Furthermore, the assumption of plane waves is not appropriate, diffraction has been ignored, and it has been assumed that there is an equal number of horizontal facets above and below the mean surface. Nevertheless, it appeared to be worth investigating the dependence on frequency ratio.

A new computer program was required and was entitled FREQCO MOD 3 (GRANDSON OF FREQCO was rejected by the computer programmer). It is described in detail in Appendix A. The

basic idea was to examine the interfrequency covariance with regard to the frequency ratio. A new normalization routine was incorporated which eliminated the frequency dependence of the source and receiver, yet still retained the $e^{-g/2}$ amplitude dependence of the sound scattered from the rough surface. This was accomplished by initially analyzing the reflected signal from a mirror surface with the aid of PRKMOD and THCDB2. The averages from THCDB2 were output on a tape which was used as one input to FREQCO MOD 3. This tape contained the mean amplitude and mean phase for each frequency for that physical setup. Runs were then made with the identical geometry but with the water surface excited by fans. It was this technique which was previously described in the section on coherence. To get the coherent amplitudes, the mean phase was required. The mean amplitude was required for normalization. After the mirror surface tape was entered, a normal THCDB2 output tape was read into the computer. Then each amplitude, for each frequency, for each time step was multiplied by the ratio of the largest average amplitude on the mirror surface tape to its own average on that tape. This arrangement, though complicated, retained the $e^{-g/2}$ dependence of the reflected amplitude. This was important because the actual effect of the rough surface, including the shift of the average amplitude, was desired. This would allow a determination of any absolute improvement to be gained by frequency switching.

The result was that the frequency response of source-receiver combination appeared flat but the rough surface acted as a low pass filter. However, the receiver still had a frequency dependent beamwidth.

The next step was to determine how the covariance of the fluctuations between two frequencies depended on the frequency ratio. From figure 20 and the simplified theory that went with it, a negative covariance was expected between a fundamental and its second harmonic when $(g)^{\frac{1}{2}}$ equaled 1.11.

The frequency ratio routine went like this. For 31 frequencies (5 kHz - 155 kHz) there are 496 possible frequency ratios from 1 to 31. Therefore, for each time step, calculate $(\Delta p_n)(\Delta p_{n+a})$ where Δp is the prèssure fluctuation relative to the mean pressure amplitude and a is the frequency increment. Also calculate $\frac{n+a}{n}$ which is the frequency ratio. Notice the sign information is again retained. Next, average each of the values for the 496 ratios over all of the time steps. Average all of the time averages where the frequency ratio is 1. Divide all of the remaining time averages by this average. This last is an attempt at normalization as in the Delta Frequency routine but it was not as effective as there were still some average covariances greater than 1. It was for this reason that the process was called a covariance rather than a correlation as in the Delta Frequency routine. In summary, the routine calculates

$$\frac{\overline{(\Delta p_n)(\Delta p_{n+a})}}{\overline{(\Delta p_1)^2}}$$

for each of up to 496 ratios of $\frac{n+a}{n}$. Finally, these values are plotted versus frequency ratio. Once again, negative covariance was desired as this would indicate the fluctuations about the mean were out of phase for the two frequencies.

Figure 21 shows the first real success of this effort. It is an analysis by frequency ratio of the same run, analyzed by delta frequency, shown in figure 18. It was over a limited range, only 5 kHz to 60 kHz, but it was consistent in that it went on for a full 2 seconds. It showed a negative covariance over the frequency ratios from approximately 2 to 4. When higher frequencies were added in, this effect disappeared. This was the first experimental indication that this negative covariance was dependent on the apparent roughness or $(g)^{\frac{1}{2}}$.

This dictated the next move, which was to try as large an angle of incidence as possible. This would give as small a $(g)^{\frac{1}{2}}$ as possible. The result was the exact geometry and electrical setup of figure 5. Figure 10 is the output of a two second run with one fan and the above setup. Figures 22, 23, and 24 are analyses of this very run by FREQCO MOD 3. The run for figure 22 used all values of amplitude and all time steps and still showed a definite negative covariance around the frequency ratio 2.

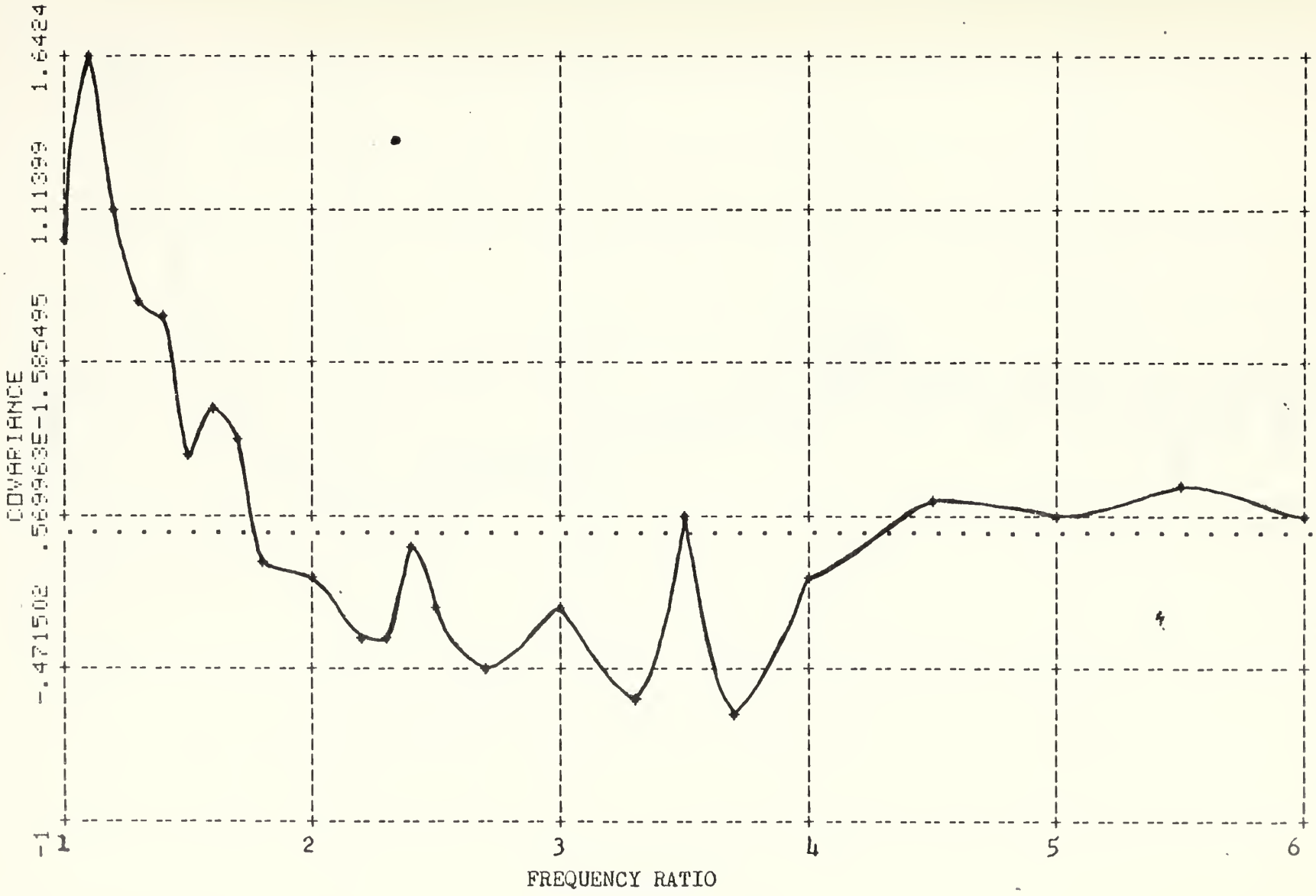

Figure 21. Interfrequency Covariance vs. Frequency Ratio.
1 Fan Surface, frequencies are 5 kHz to 60 kHz over 2 seconds.
Angle of incidence 32.6°.

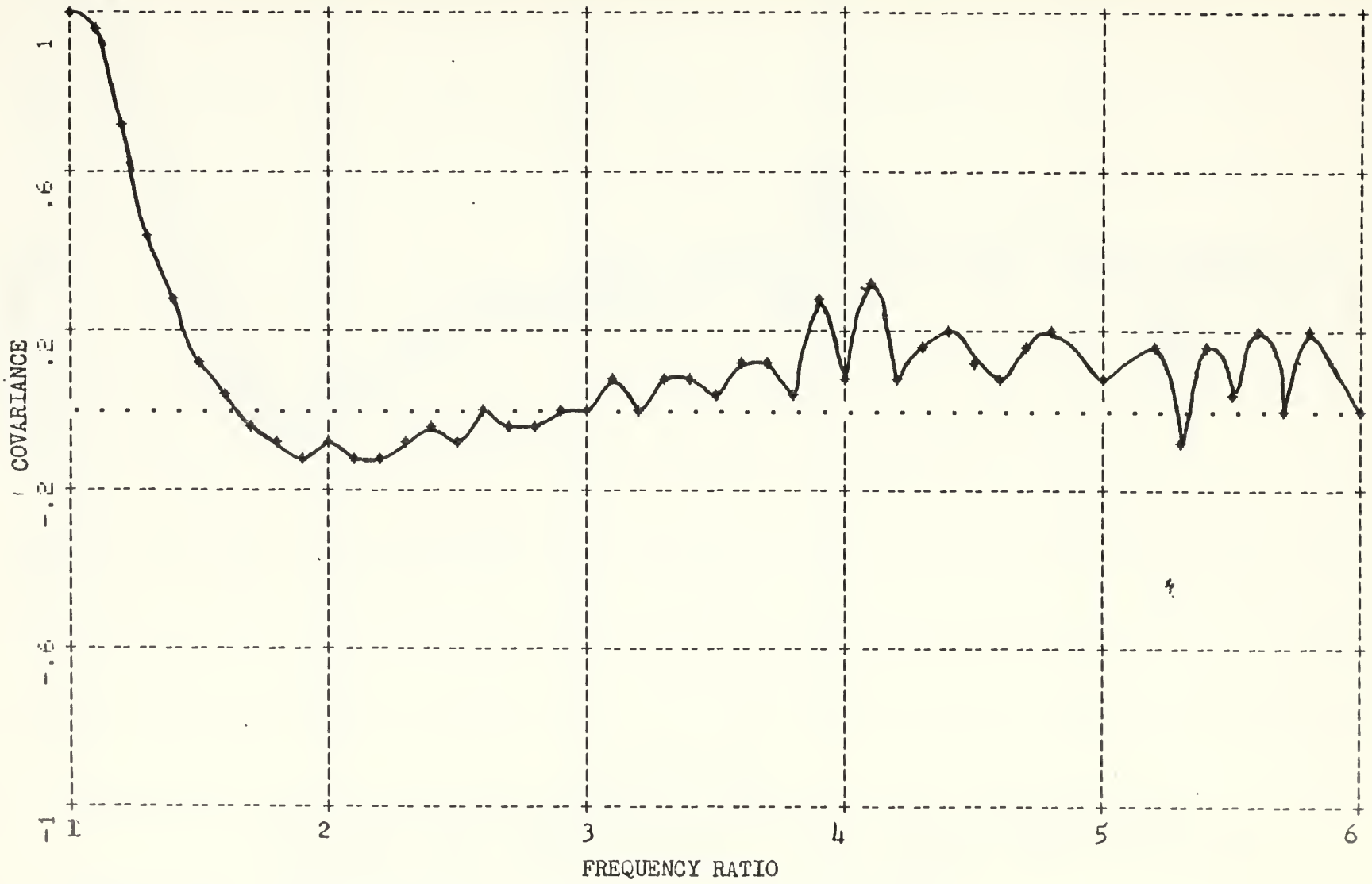

Figure 22. Interfrequency Covariance vs. Frequency Ratio
1 Fan Surface, Frequencies are 5 kHz to 155 kHz over 2 seconds.
Angle of incidence 66.1°

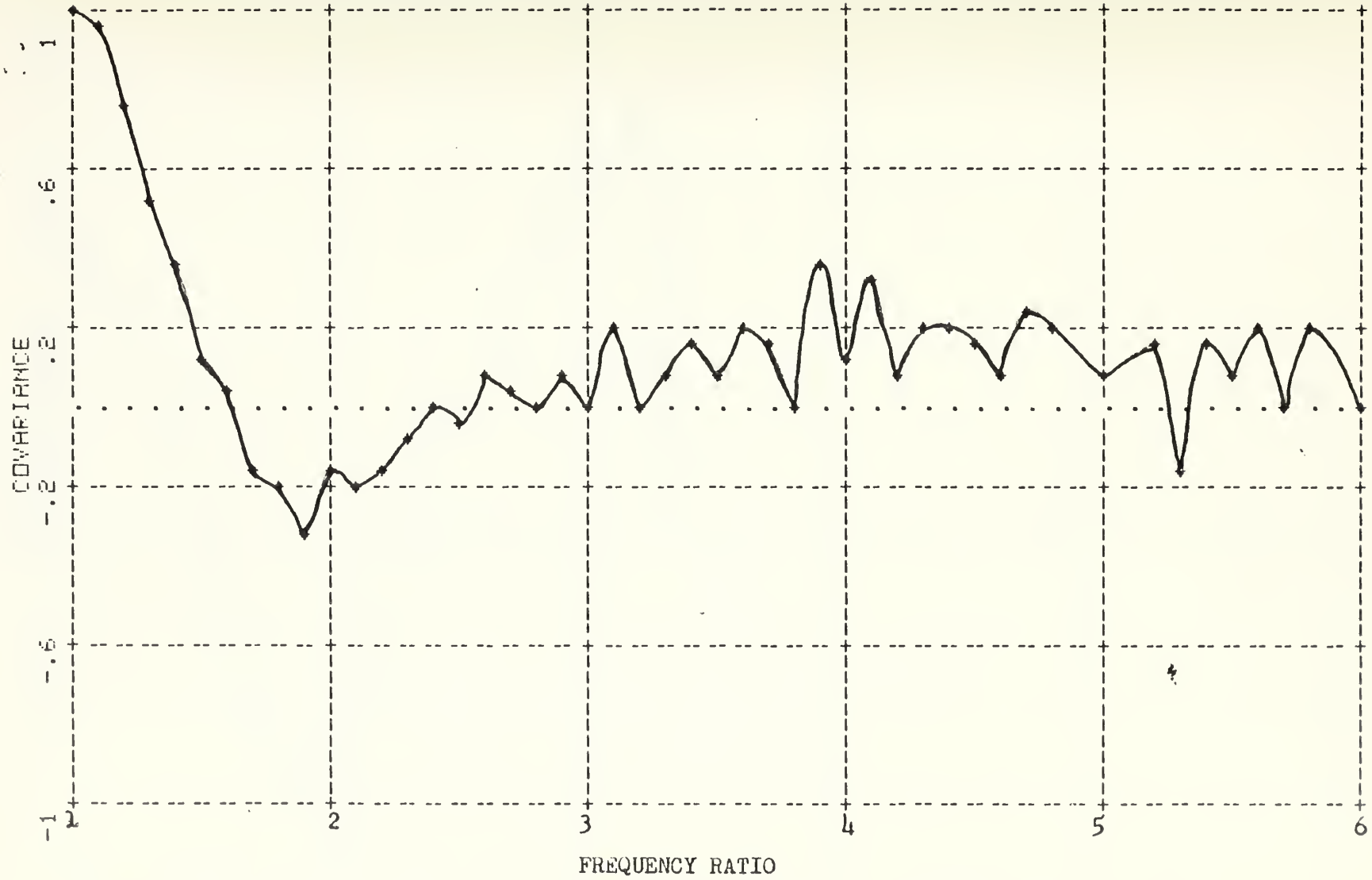

Figure 23. Interfrequency Covariance vs. Frequency Ratio evaluated when lower freq. is below its mean. 1 fan surface, freqs. are 5 kHz to 155 kHz over 2 seconds. Angle of incidence 32.6°.

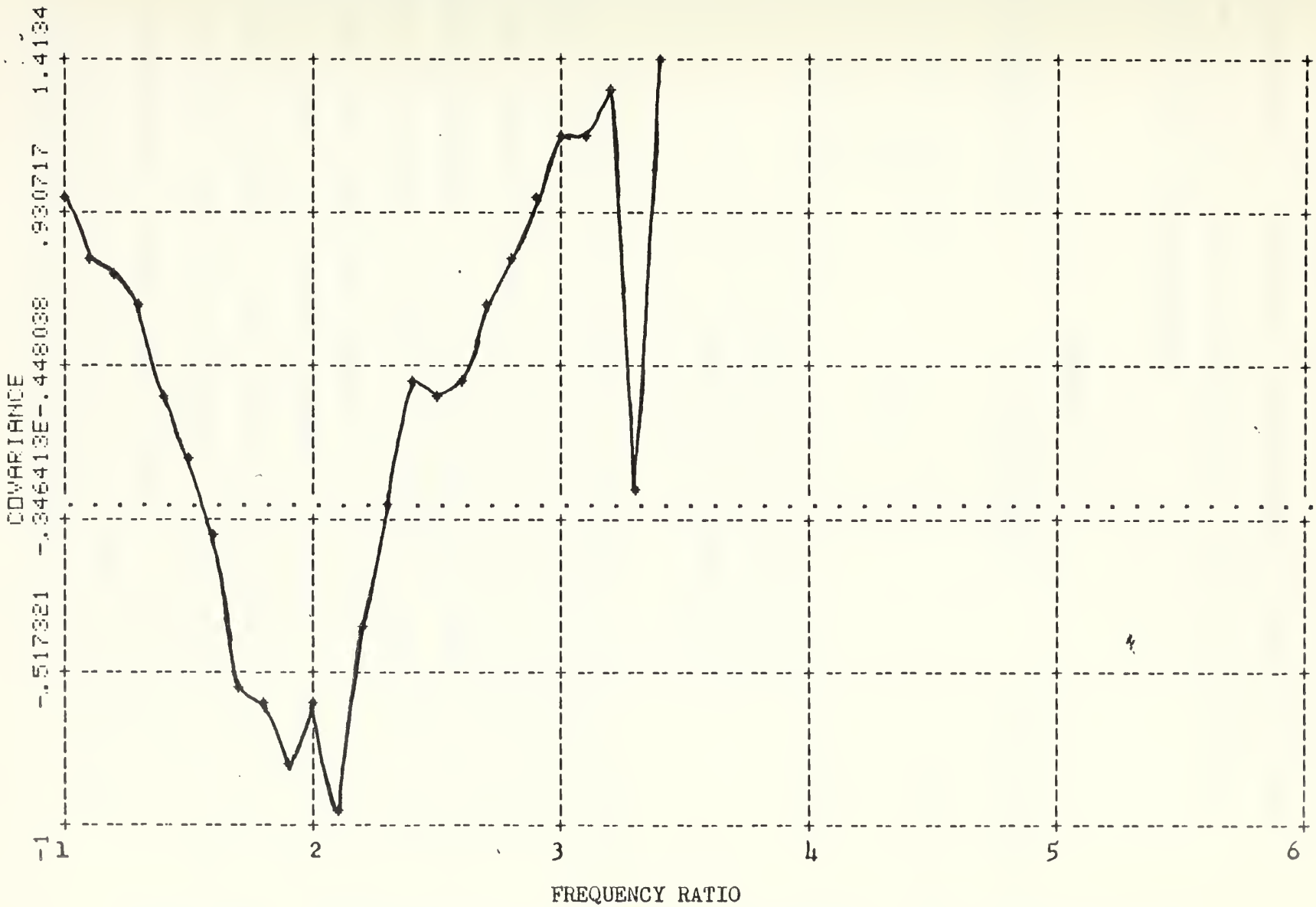

Figure 24. Interfrequency Covariance vs. Frequency Ratio evaluated when lower freq. is more than 3 dB below its mean. 1 fan surface, freqs. are 5 kHz to 155 kHz over 2 seconds. Angle of incidence 32.6°

The next objective was to try to improve the negative covariance by selectively performing the operation over certain time ranges or bandwidths. This would explain more about the phenomenon.

TABLE III

PATH DIFFERENCE FOR f_1		PATH DIFFERENCE FOR $2*f_1$		PATH DIFFERENCE FOR $3*f_1$	
$\lambda/2$	(D)	λ	(C)	$3\lambda/2$	(D)
λ	(C)	2λ	(C)	3λ	(C)
$3\lambda/2$	(D)	3λ	(C)	$9\lambda/2$	(D)

C = CONSTRUCTIVE INTERFERENCE

D = DESTRUCTIVE INTERFERENCE

Referring now to figure 20 and table III it is apparent that, depending on the frequency, there can sometimes be constructive interference for both the fundamental and the second harmonic. This would reduce the negative covariance. For this reason, an option was added to FREQCO MOD 3 which caused the covariance operation to be performed only if the amplitude of the lower frequency was below a certain percentage of its mean. This certain percentage of the mean is called the "switching threshold". This was the more realistic situation as the only time one would consider switching to a higher frequency would be if the lower frequency was experiencing destructive interference.

Figures 23 and 24 analyze the same run as figure 22 but utilize different switching thresholds. Once again this is the run used as an example in figure 10. Figure 23 uses the mean of the amplitude of the lower frequency (f_1) as the switching threshold, while figure 24 uses 3 dB below the mean. Obviously, dramatic changes in the negative covariance will result with a change in switching threshold but the minimum is still right around two. The dashed lines in figure 10 show the 3 dB below the mean value when it is present. It is apparent that for this run there are not many points more than 3 dB below the mean, but where there are some, the double frequency always has a peak. Figure 24 cuts off at a frequency ratio of 3.4 because the lowest frequency to have any points 3 dB below its mean is 45 kHz and 155/45 = 3.4. Notice also that figure 24 shows a strong positive covariance at the frequency ratio of 3. This is as predicted by the calculations shown in table III.

F. SHORT TERM VARIABILITY OF RMS WAVE HEIGHT

It had become apparent that the negative covariance showing up at a frequency ratio of 2:1 was very dependent on effective surface roughness or g. To this point, the long term RMS wave height calculated by Loomis (Ref. 8) had been used in the calculation of g. When the data for many different runs were broken down into covariances for different frequencies, the dependence on g could be calculated. This was attempted but little agreement was arrived at

concerning dependence on g. One question that came to mind was whether the long term RMS height should be used in the calculation of g. To determine this, five identical two second runs were made. Theory says that

$$\ln \frac{\langle p \rangle}{p_o} = - g/2.$$

So $\frac{\langle p \rangle}{p_o}$ was calculated and plotted on semi-logarithmic paper versus (frequency)^2 for these five runs. Figure 25 is a compilation of these plots. All are two second runs in a two fan sea and the angle of incidence was 44.1°. The only thing that could account for the large changes in these slopes would be a large variability in the RMS wave height from one run to the next. From the slope of each of these curves one could calculate an RMS wave height; the ratio of the largest to the smallest was over 2:1.

It was decided to determine whether this type of variability was possible by observing a series of two second studies of the RMS height of our statistically stationary surface. Therefore the circuit of figure 26 (from Loomis) was rigged. It utilizes a wave probe whose capacitance is determined by the water depth to which the probe is immersed. The probe is connected to the impedance bridge shown in figure 26. The impedance bridge has a convenient feature in that it provides a 1 kHz output modulated by the value of the input capacitance. As the probe depth is varied by the wave action, the final signal provides a linear output proportional

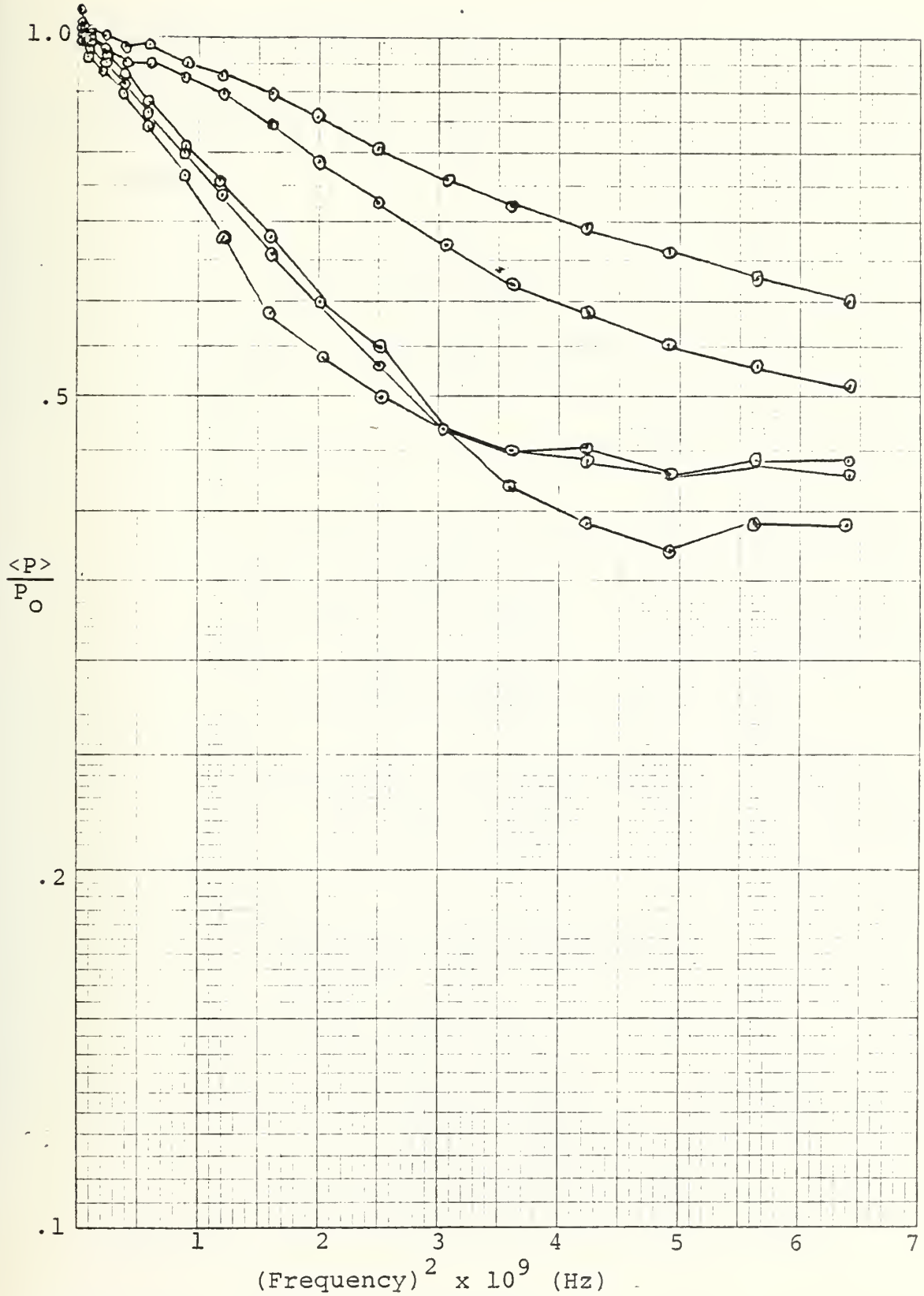

Figure 25. ln $\frac{<P>}{P_o}$ vs. (frequency)^2
All are 2 second runs.

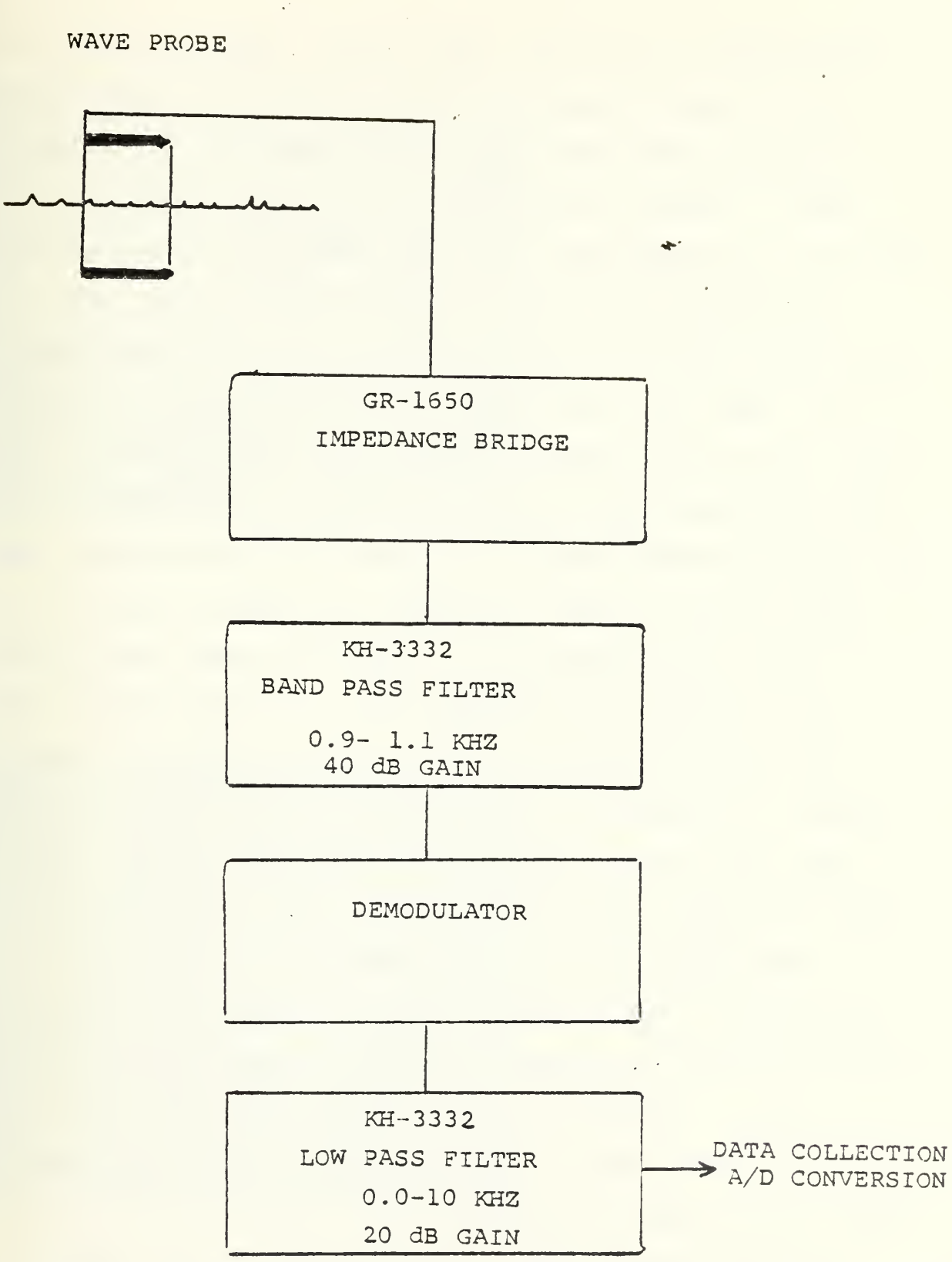

Figure 26. Wave Height Data Collecting Circuit

to the probe depth. This output was led to a persistence scope where the pictures shown in figures 27 and 28 were taken. Each of these photos is a linear representation of the surface height that existed over two seconds. These photos were two extremes taken over approximately 10 minutes of time, but the wave height in figure 28 is more than three times the wave height in figure 27. This alone establishes the variability, but another check was made. CAL-01 is a program which gives the RMS voltage of any input signal. It is described in appendix A. CAL-01 analyzed about fifty, two second runs and of these the largest RMS wave height was 3.45 times the smaller. Obviously, the variation in RMS wave height shown by figure 25 is reasonable for runs of two second duration. It is important to remember that these two second runs translate into approximately five ocean wave periods and approximately 50 seconds of "ocean time". Thus to determine the correct g for any run, the actual RMS height must be determined from a graph like that of figure 25. It is known that longer runs show less variability. Figure 29 shows this is correct. These five runs were made under conditions identical to those of figure 25 except they were looked at for six seconds. It is immediately obvious that they have a tighter distribution than the five previous two second runs. Thus the RMS height of these runs is approaching the long term RMS height of the model ocean.

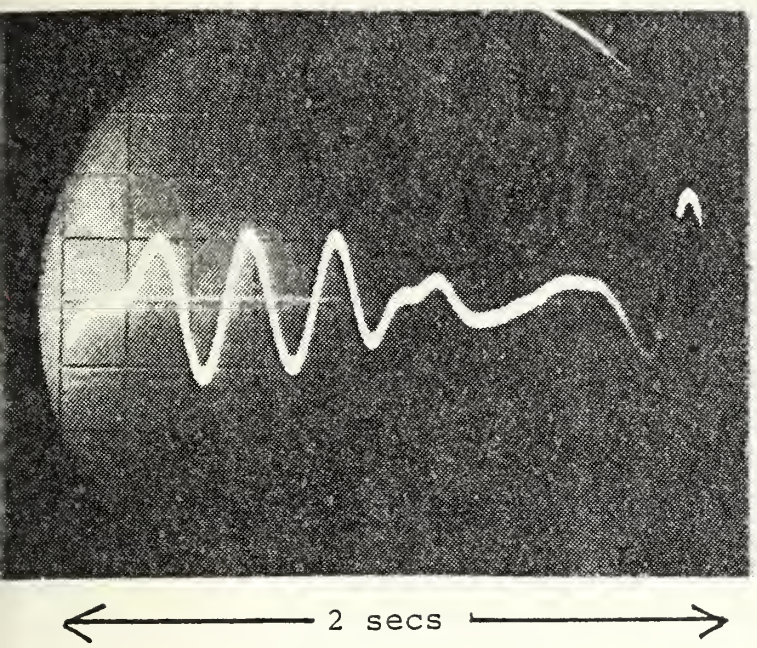

Figure 27.

Wave Height vs. Time on a persistence scope. Example of very small wave height.

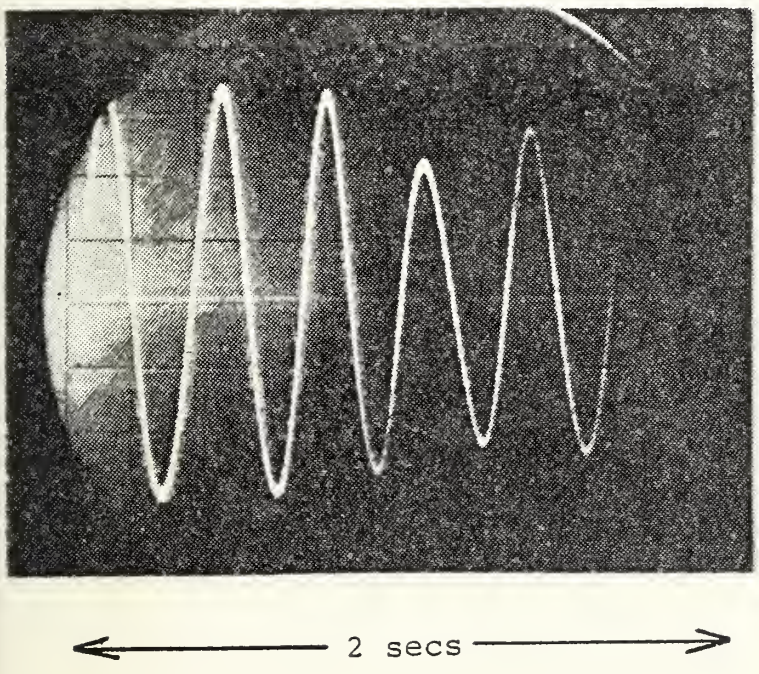

Figure 28.

Wave Height vs. Time on a persistence scope. Example of very large wave height.

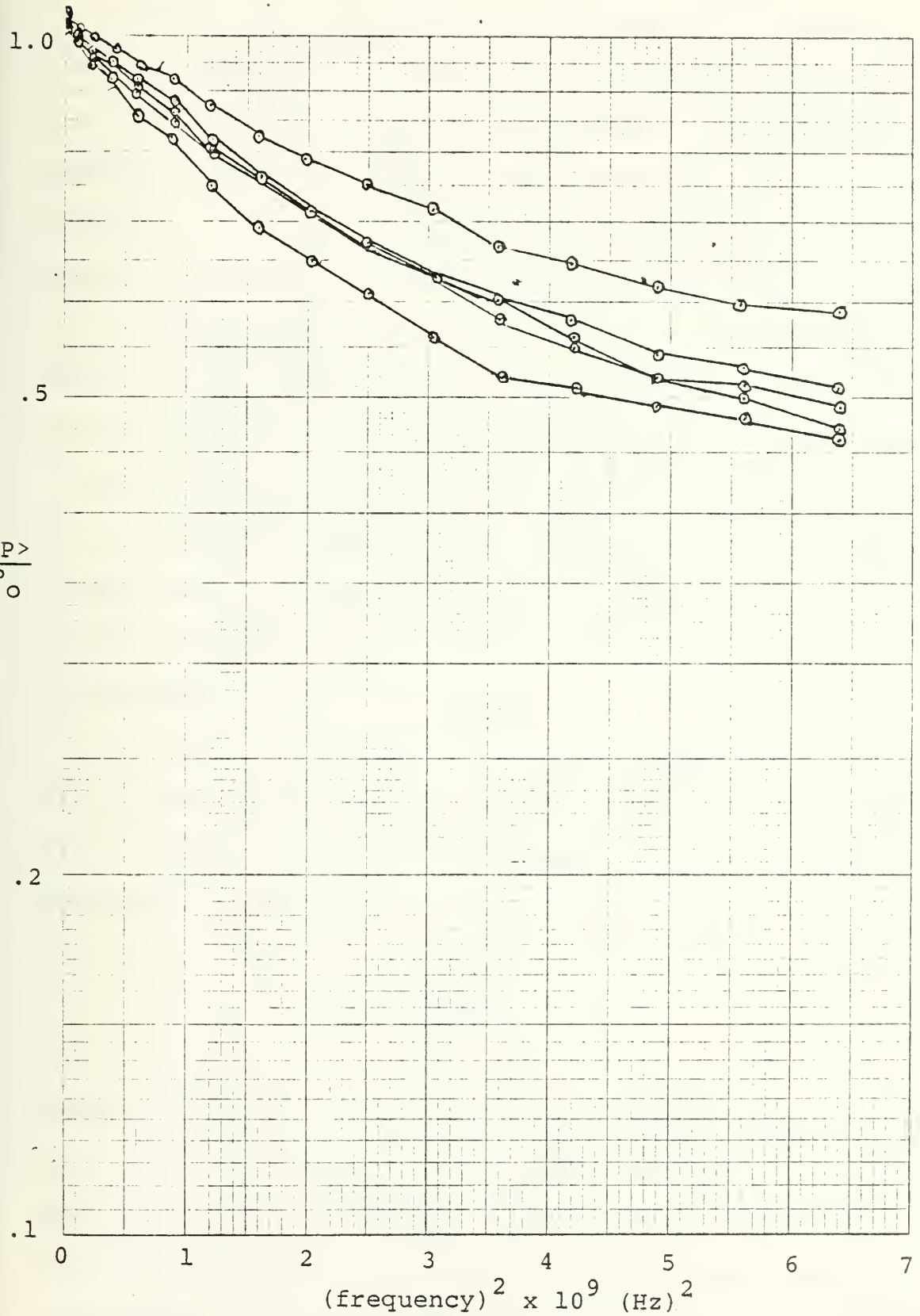

Figure 29. ln $\frac{<P>}{P_o}$ vs. (frequency)^2
All are 6 second runs.

G. SIGNAL ENHANCEMENT DUE TO FREQUENCY SWITCHING

It had been established by now that the frequency ratio of 2:1, especially in the low roughness situations would give a significant negative covariance. The question to be answered next was whether it ever would be profitable to switch to a higher frequency. There would have to be a very good reason to do this because of the greater absorption loss at the higher frequencies, as well as the added scattering loss off of a rough surface for higher frequencies. The increased absorption of higher frequencies was not looked at during these efforts but it might be a limiting factor to any practical application. However, because of the normalization process described for FREQCO MOD 3, the greater scattering loss for higher frequencies was retained in the processing.

The signal enhancement routine of FREQCO MOD 3 provides the ability to determine the gain in dB provided by switching from a fading frequency of interest to its second harmonic. The gain is defined as:

$$20 \log\left[\frac{\int p_2 \, dt}{\int p_1 \, dt}\right]$$

where p_1 is the pressure of the fundamental frequency f_1 and p_2 is the pressure of the second harmonic, $f_2 = 2*f_1$. The integration is performed only when p_1 is less than the switching threshold. Determining the RMS wave height for a particular run in the manner described in the last section

allows one to calculate a $(g)^{\frac{1}{2}}$ for every lower frequency f_1. Gain in dB may then be plotted against the $(g)^{\frac{1}{2}}$ of that frequency. Figure 30 is the result of this type of analysis. It is the average of 12 different two second runs taken at different angles of incidence, with different numbers of fans and all using the mean of the amplitude of f_1 as the switching threshold.

The data of all 12 runs fit very well together especially in the region below $(g)^{\frac{1}{2}} = 1.0$. There was a very stable gain of about 0.9 dB in the region where $(g)^{\frac{1}{2}} = 0.25$. However, there was a loss of 2.4 dB using this technique in the region where $(g)^{\frac{1}{2}} = 0.65$. The best gain is at $(g)^{\frac{1}{2}} = 1.45$ where it is 1.4 dB. There is a gain experienced in the entire region from $(g)^{\frac{1}{2}} = 0.9$ to 1.8. The data base drops off with increasing $(g)^{\frac{1}{2}}$ since most runs were taken at smaller effective roughnesses. There are still 7 runs active at $(g)^{\frac{1}{2}} = 1.45$, though. Another point to be made is that each of these runs actually is an average itself of about 50 points. Thus, where 7 runs are averaged, there is a total data base of about 350 points.

Figure 31 shows a comparison of gain vs. $(g)^{\frac{1}{2}}$ for the same two second runs in figure 30 compared to five other six second runs. Both use the mean amplitude of f_1 as the switching threshold. It appears that the gain above $(g)^{\frac{1}{2}} = 1.0$ is very sensitive to the RMS wave height. If one accepts the idea of "wave packets" of similar characteristics traveling in groups of three to five (Ref. 6) one could

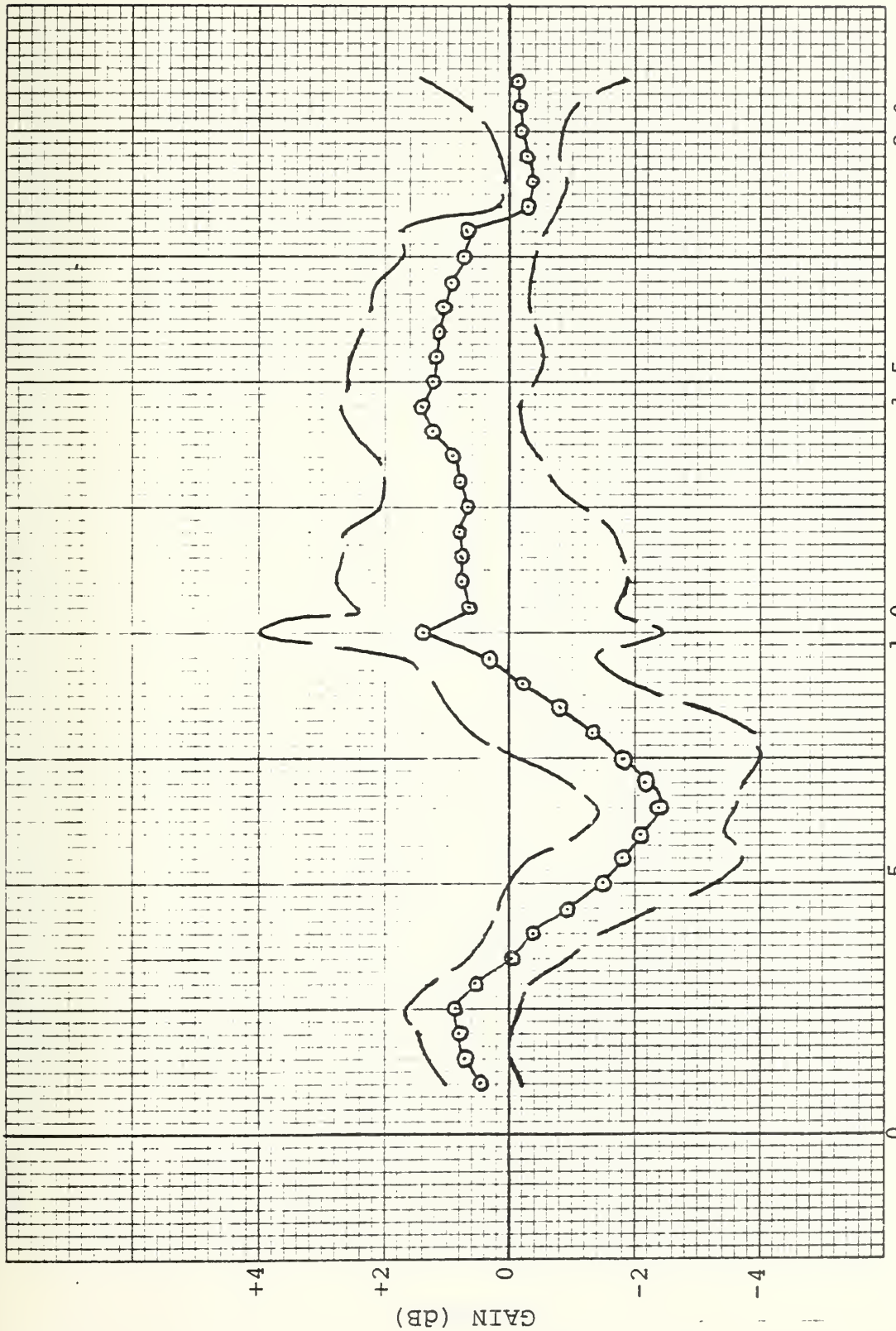

Figure 30. Gain vs. $(g)^{\frac{1}{2}}$ for voltages using mean as a switching threshold. Dashed lines show one standard deviation. Twelve, two second runs.

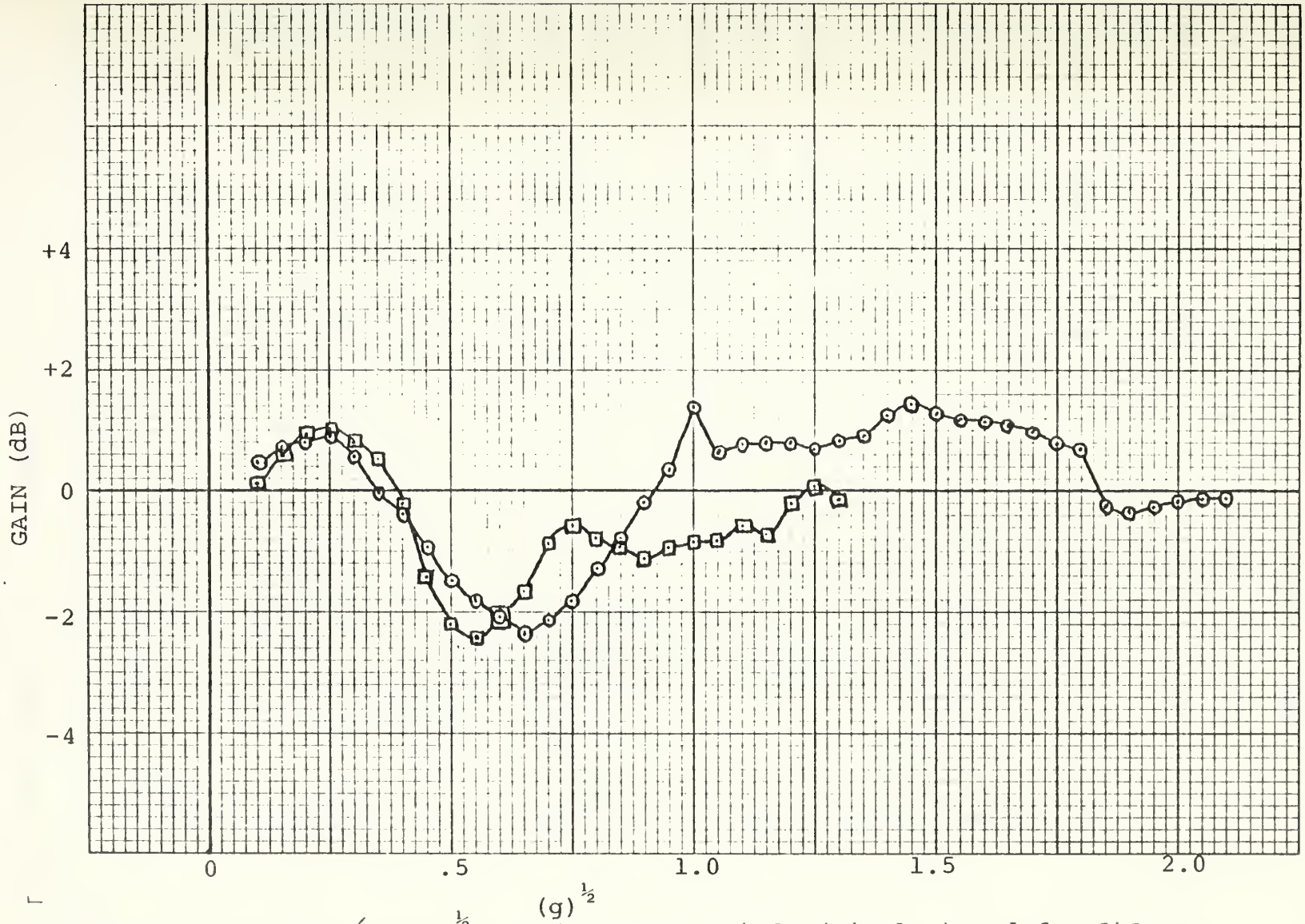

Figure 31. Gain vs. $(g)^{\frac{1}{2}}$ for five wave periods (circles) and for fifteen wave periods (squares). Both using mean as switching threshold.

account for the disappearance of the gain at $(g)^{\frac{1}{2}}$ greater than 0.9. Perhaps each of these six second runs was composed of several different wave packets. Then the RMS height of each of these wave packets would be different. This would cause the minimum at $(g)^{\frac{1}{2}} = .65$ to oscillate back and forth through a range of frequencies as the RMS wave height changed. This would obliterate any gain in the region of large $(g)^{\frac{1}{2}}$ and might give a curve like that of the squares in figure 31. It is interesting that the gain at $(g)^{\frac{1}{2}} = .25$ is very stable even for the longer term runs.

Figure 32 shows the effect of using the coherent amplitudes rather than the total amplitudes of the same 12 runs as in figure 30. Again both use the mean of the lower frequency as the switching threshold. This technique reduces the gain slightly around $(g)^{\frac{1}{2}} = 0.25$ but it increases the gain from $(g)^{\frac{1}{2}} = 1.35$ on up. The run with the circles is the standard from figure 30. The data base is 2 runs above $(g)^{\frac{1}{2}} = 2.0$ but it is still 7 runs at $(g)^{\frac{1}{2}} = 1.45$ where this technique adds 0.4 dB. It apparently is the coherent component which sees this effect most strongly.

In figure 33, the effect of changing the switching threshold is investigated. The circles are the averages of the 12 runs from figure 30 with a switching threshold of the mean amplitude at f_1. The squares are the same 12 runs but the switching threshold is 3 dB below the mean amplitude at f_1. The curves are roughly parallel but the increase in the gain is dramatic. The overall percentage

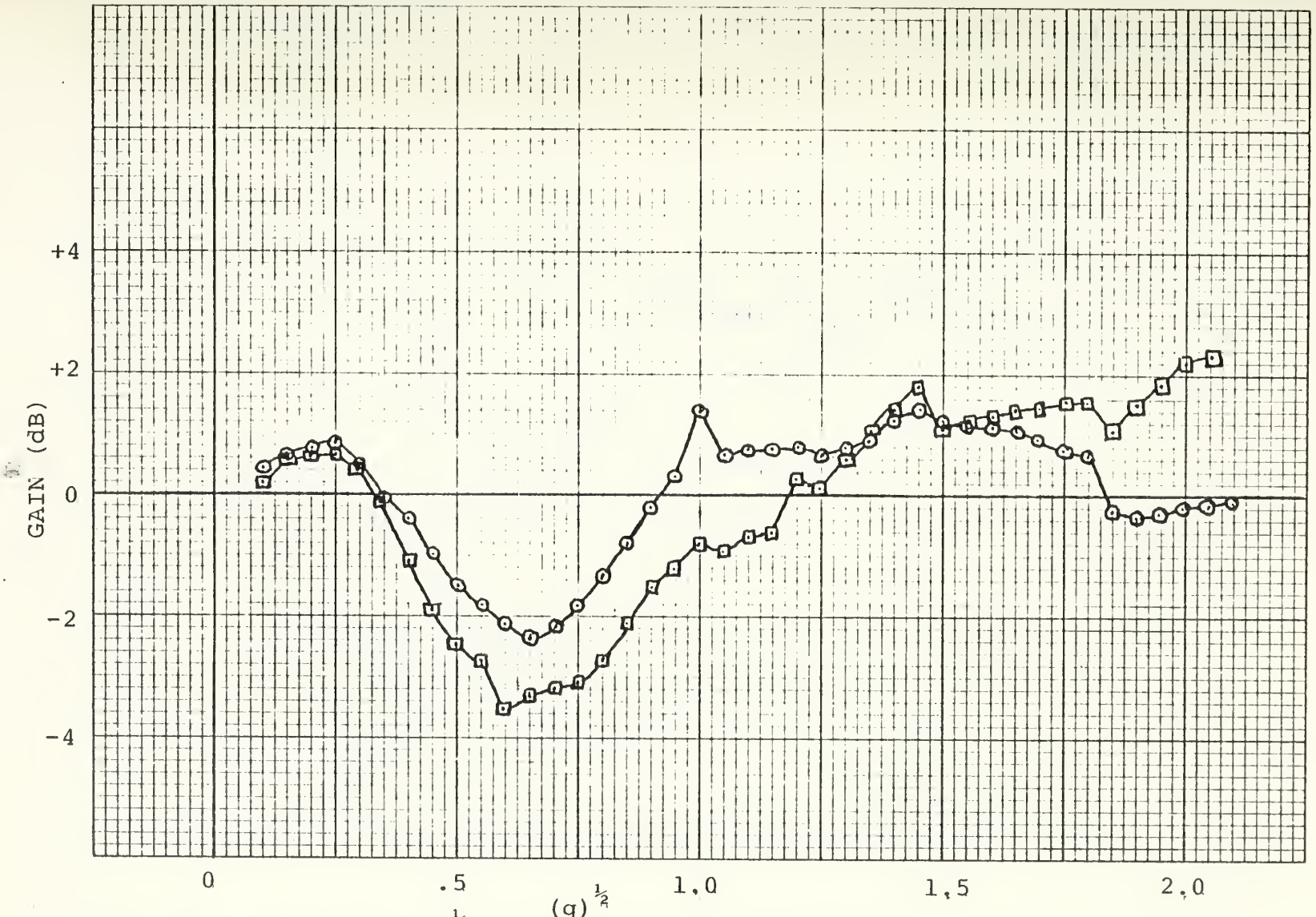

Figure 32. Gain vs. $(g)^{\frac{1}{2}}$ for coherent voltages (squares) and for total voltages (circles). Both using mean as switching threshold. Standard deviations similar to those of Figure 30.

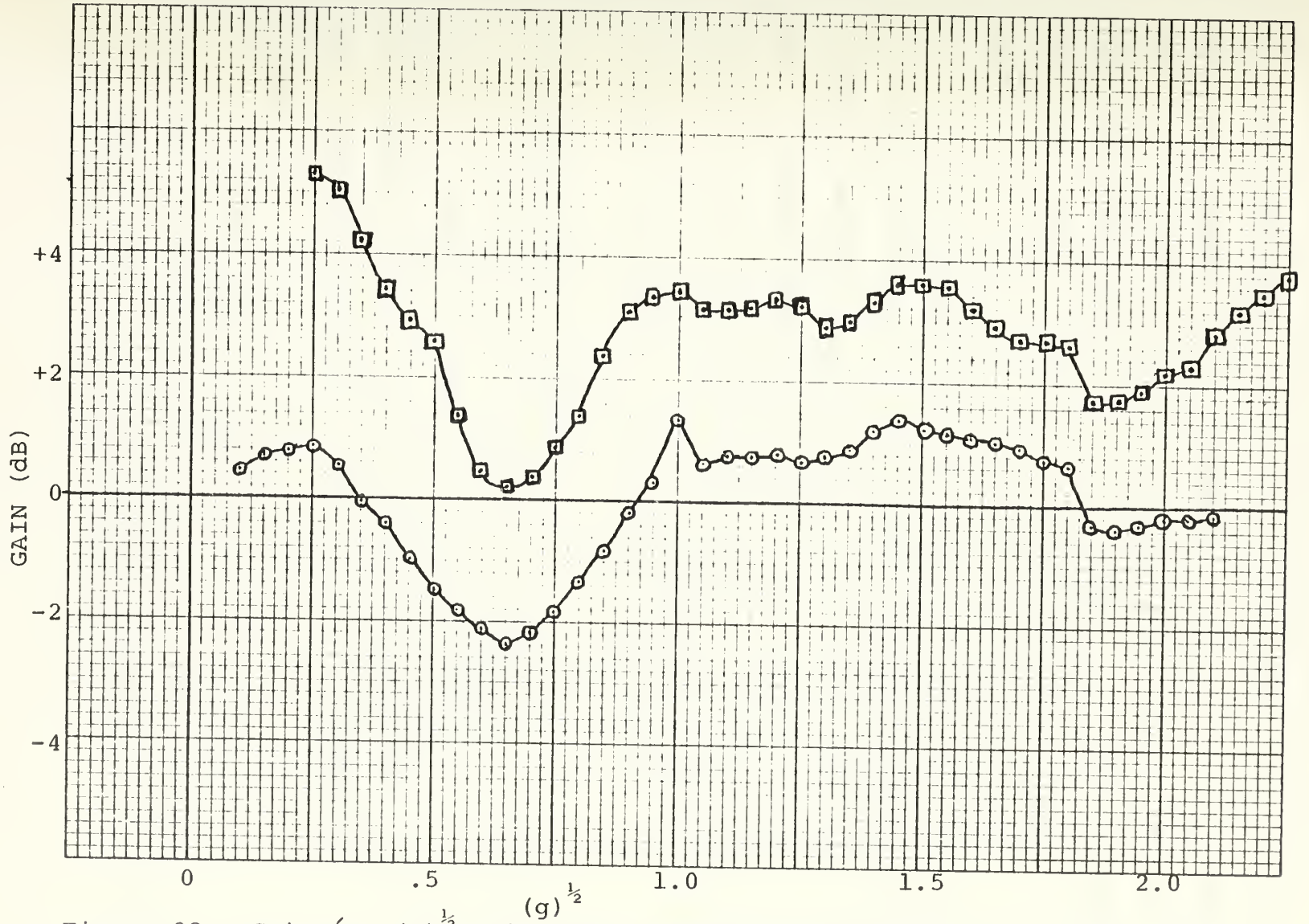

Figure 33. Gain vs. $(g)^{\frac{1}{2}}$ using mean as switching threshold (circles) and using 3 dB below mean as a switching threshold (squares). Standard deviations similar to those of Figure 30. Each has twelve, two second runs.

of time during which the amplitude is below the switching threshold for the upper curve in this figure is 20% as compared with about 50% for the lower curve. For the smaller effective roughnesses in the upper curve it is approximately 10% but it grows rapidly to 30% for the higher effective roughness, then stays constant. Thus it is apparent that sizeable gains can be made in signal processing just by switching to the second harmonic at the proper time.

It is interesting to note here that the simple model of figure 20 along with the mathematics for a sinusoidal surface predicted a cancellation effect and subsequent gain for the second harmonic at $(g)^{\frac{1}{2}} = 1.11$. Here, with a Gaussian surface the maximum consistent gain occurred at $0.9 < (g)^{\frac{1}{2}} < 1.8$. The smaller steady gain of about 0.9 dB at $(g)^{\frac{1}{2}} = 0.25$ was not predicted by this method.

H. RESULTS AND CONCLUSIONS

1. Over a certain effective roughness or $(g)^{\frac{1}{2}}$ region there is a definite anti-correlation between a signal and its second harmonic. This anti-correlation increases as the "switching threshold" of the primary frequency is lowered.

2. Within certain roughness regions, significant dB gains can be made by switching from the fundamental to its second harmonic. The amount of gain depends critically on the switching threshold.

3. The coherent component of the voltage provides greater gain for higher roughnesses.

4. There appears to be a time dependence of the gain especially for higher roughnesses. High gains were obtained for runs on the order of 5 ocean wave periods (approximately 50 seconds of "ocean time"). The gain for higher roughnesses vanishes for longer runs on the order of 15 ocean wave periods (150 seconds of "ocean time"). However, the gain at $(g)^{\frac{1}{2}} = .25$ was steady even for the longer duration runs.

5. There does not appear to be any dependence of gain on the angle of incidence in the range used (24.3° to 66.1°) as long as the results are plotted against $(g)^{\frac{1}{2}}$.

VI. RECOMMENDATIONS FOR FUTURE RESEARCH

Further investigation should provide additional information. Several avenues of approach are:

1. Expand the data base. Data taking was limited by the storage capability of OPHELEA. With the addition of a floppy disk, the situation should be improved and a greater data base could be created.

2. Determine if this effect will exist through multiple bounces from the rough surface. A possible method could be recording of the reflected signal and bouncing it off the surface again, examining it the second time.

3. Investigate the effect that parallel processing of the signals would have as opposed to switching back and forth.

4. An at sea experiment, controlled to allow only one surface reflection would be useful. The simultaneous transmission of several pairs of fundamentals and second harmonics would verify the dependence on g.

APPENDIX A

COMPUTER PROGRAM DESCRIPTIONS

PRK-MOD

Program to perform A/D sampling on one channel. There is an adjustable delay between each block of samples. The program also discards the first block to avoid the problem of starting to sample in the middle of a block. The output is written on a digital cassette which can be used as the input for THCDB1 and THCDB2 and PRKPLOT.

Input:
1. Number of blocks
2. Number of points per block as a power of two. (Total number of points must be less than 13000)
3. Time delay between blocks
4. Sample frequency

Output: Raw A/D data stored on digital cassette.

THCDB1:

Program to convert raw A/D data into a frequency spectrum for every 5 kHz from D.C. to 160 kHz. This program assumes sampling at 320 kHz. The block size may be from 64 to 2048 samples, though the frequency resolution is always 5 kHz.

Input:
1. Number of sample points per block as a power of two
2. Total number of FFT's desired (maximum of 100)

3. Conversion factor for transforming PSD to volts
4. Amplifier gain
5. Line loss
6. Hydrophone sensitivities for every 5 kHz from 0 to 160 kHz

Options:
1. SPL or VL output
2. Noise run

Output:
1. Mean sound pressure level (or voltage level) vs. frequency
2. Standard deviation of SPL vs. frequency
3. Signal to noise ratio vs. frequency if previous noise run has been performed
4. SPL or VL for each individual run
5. Output can be stored on digital cassette or printed on the terminal printer.

THCDB2:

Program to convert Raw A/D data into a frequency spectrum for every 5 kHz from D.C. to 160 kHz. The program assumes sampling at 320 kHz. The block size may be either 64 or 128 samples. The resolution is always 5 kHz. Phase information is also provided.

Input:
1. Number of sample points per block as a power of two
2. Total number of FFT's desired (maximum of 100)
3. Conversion factor for transforming PSD to volts

Options: 1. Output averages to tape or printer

Output: 1. Mean voltage level vs. frequency

2. Standard deviation of voltage level vs. frequency

3. Mean phase vs. frequency

4. Standard deviation of phase vs. frequency

5. Voltage levels and phase vs. frequency for each time step

6. Coherent voltage levels and phase vs. frequency for each time step.

Note: 1. Mean phase avoids the π, $-\pi$ radian discontinuity in the following manner: If the absolute value of the phase for a particular frequency for any time step is greater than 2.5 radians, 2π radians are added to each negative value of the phase. The average is then calculated. This technique works well when the phase distribution is fairly tightly grouped.

2. Coherent voltages are calculated in the following manner:

$$\text{Coherent Volts} = \text{Volts} \times \left|\cos(\text{Average Phase} - \text{Instantaneous Phase})\right|$$

CAL-01:

Input:
1. Number of samples (maximum 8192)
2. Input reference voltage set at 1.00 volts (RMS)
3. Voltage signal from wavetank probe

Output:
1. VOUT = AC voltage or wavetank probe

PRKPLOT (BASIC):

Input:
1. Output tape of PRKMOD

Options:
1. Ability to only plot every n^{th} point

Output:
1. Plot of raw A/D data

SORTPLOT (BASIC):

Input:
1. Output tape of THCDB2
2. Bandwidth for plot
3. Number of time steps
4. Amplitude and/or phase plots

Output:
1. Plots of amplitude and/or phase vs. time

HISTOGRAM:

Input:
1. OUtput tape of THCDB2
2. Bandwidth of interest
3. Number of time steps
4. Amplitude and/or phase histograms

Output:
1. Plots of amplitude and/or phase histograms

SON OF FREQCO (BASIC):

Input:
1. Output tape of THCDB2
2. Bandwidth of interest

3. Number of time steps

Options: 1. Normalization option (The values for each frequency are multiplied by the ratio of the max. pressure mean to its own mean)

2. Calculate means or input them from keyboard

Output: 1. Plot of frequency correlation vs. delta frequency

FREQCO MOD 3:

Input: 1. Output tape of THCDB2

2. Number of time steps

3. Bandwidth of interest

4. Ratio of interest

5. RMS Waveheight

6. Grazing angle

7. Fraction of mean of lower frequency below which operations will take place. (To use all values make this a large number)

Options: 1. Normalization option (To use this, an output tape of THCDB2 averages must be input when called for. This tape should have been made with a mirror surface. Then each value for each frequency is multiplied by the ratio of the maximum mean pressure from this tape to its own mean on this tape.)

2. Change voltages to coherent voltages with the same routine as that of THCDB2 except that the mean values of phase are taken from the input mirror surface tape
3. Only perform signal enhancement routine. This routine computes the ratio of p_2 to p_1 only when p_1 is below its mean and takes 20 times the log to base 10 of it.

Output:
1. Value of $g^{\frac{1}{2}}$ for lower frequencies and covariance between these and the upper frequencies. The upper frequencies depend on the ratio of interest previously input. The covariance is calculated only when the amplitude of the lower frequency is below the fraction of the mean previously input.
2. Plot of covariance vs. frequency ratio.
3. Output of signal enhancement routine which is the gain in dB for switching from p_1 to p_2 when p_1 is below its mean.

BIBLIOGRAPHY

1. Medwin, H, "Specular Scattering of Underwater Sound from a Wind Driven Surface," The Journal of the Acoustical Society of America, v. 41, p. 1485-1495, 1967.

2. Clay, C.S., Medwin, H., and Wright, W.M., "Specularly Scattered Sound and the Probability Density Function of a Rough Surface," The Journal of the Acoustical Society of America, v. 53, pp. 1677-1682, 1973.

3. Tolstoy, I., and Clay, C.S., Ocean Acoustics: Theory and Experiment in Underwater Sound, McGraw-Hill, 1966.

4. Beckmann, P., and Spizzichino, A., The Scattering of Electromagnetic Waves From Rough Surfaces, MacMillan, New York, 1963.

5. McDonald, J.F., Tuteur, F.B., and Zoring, J.G., "Spatial Interfrequency Correlation Effects in a Surface-Scatter Channel," The Journal of the Acoustical Society of America, v. 59 pp. 1284-1293, 1976.

6. Perkins, J.B., Amplitude Modulation of Acoustic Signals by Ocean Waves and the Effect on Signal Detection, M.S. Thesis, U.S. Naval Post Graduate School, 1974.

7. Tourville, M.A., Signal Enhancement of Surface Scattered Underwater Sound, M.S. Thesis, U.S. Naval Postgraduate School, 1975.

8. Loomis, M.F., Frequency Time Correlation of Surface Scattered Underwater Sound, M.S. Thesis, U.S. Naval Postgraduate School, 1976.

9. Thomas, J.B., An Introduction to Statistical Communication Theory, Wiley, 1969.

INITIAL DISTRIBUTION LIST

		No. Copies	
1.	Library, Code 0142 Naval Postgraduate School Monterey, California 93940	2	
2.	Department Chairman, Code 61 Department of Physics and Chemistry Naval Postgraduate School Monterey, California 93940	2	
3.	Professor H. Medwin, Code 61Md Department of Physics and Chemistry Naval Postgraduate School Monterey, California 93940	6	
4.	Lt. Robert B. Shields, Jr. 1619 Centre Street Newton, Mass. 02161	1	
5.	Manager Anti-Submarine Warfare Systems Project Office Attn: Capt. D. Elliot Department of the Navy Washington, D.C. 20360	1	
6.	Professor J. Novarini Av. Cordoba 4190 1188 Cap. Fed. Buenos Aires Argentina	1	
7.	Director of Defense Research and Engineering Office of the Secretary of Defense Washington, D.C. 20301 ATTN: Office, Assistant Director (Research)	1	
** 8.	Defense Documentation Center Cameron Station Alexandria, Virginia 22314	12	**
9.	Director Naval Research Laboratory Washington, D.C. 20375 ATTN: Library, Code 2620	6	

		No. Copies
10.	Office of Naval Research Arlington, Virginia 22217	
	ATTN: (Code 480)*	3
	ATTN: (Code 460)	1
	ATTN: (Code 102-OS)	1
	ATTN: (Code 102IP)	6
11.	Commander Naval Oceanographic Office Washington, D.C. 20390	
	ATTN: Code 1640	1
	ATTN: Code 70	1
12.	NODC/NOAA Rockville, MD 20882	1

* Add one separate copy of Form DD-1473

** Send with these 12 copies two completed forms DDC-50, one-self addressed back to contractor, the other addressed to ONR, Code 480

Thesis
S4675
c.1

174008

Shields
Signal enhancement
of specularly scat-
tered underwater sound.